TEST-CASE: HPP Schiffmühle, Switzerland

Prepared by Ismail Albayrak[1,1], Muhammadreza Maddahi[1], Cristina Rachelly[1], Martin Detert[1], Robert Boes[1], Armin Peter[2], Christian Milzow[3,] Jeffry Tuhtan[4], Kordula Schwarzwälder[5], Nils Ruther[5], Andreas Doessegger[6]

[1]VAW, ETH Zurich, [2]FCO, [3]AF-Consult, [4]TUT, [5]NTNU and [6]LKW

[1,1]Responsible person: albayrak@vaw.baug.ethz.ch

Table of Contents

Figures

Tables

1 Description of the Test-Case

1.1 Description of the water bodies related to the HPP

The residual flow and main run-of-river hydropower plant (HPP) Schiffmühle are located on the 35 km long river Limmat in Untersiggenthal and Turgi near Baden, some 27 km downstream of Lake Zurich. Between Lake Zurich and Schiffmühle there are seven HPPs, namely in flow direction Letten, Höngg, Dietikon, Wettingen, Aue, Oederlin and Kappelerhof (Fig.1). There are three more power plants between HPP Schiffmühle and the junction with river Aare, namely Turgi, Gebenstorf and Stroppel. Altitudes of the lowest and highest points of river Limmat are 330 m and 406 m asl, respectively, resulting in an average bed slope of 2.2 per mil. The surface area of the whole catchment amounts to 2384 km^2, of which 0.7 % are glaciated.

Figure 1: Water bodies related to the HPP Schiffmühle

1.1.1 Hydrology of river Limmat

On river Limmat, the mean monthly discharge increases from March to June and then decreases until autumn (Fig. 2). The mean annual discharge in 2015 was 89 m^3/s (Fig. 2), while the long-term average is 101 m^3/s (1951-2015).

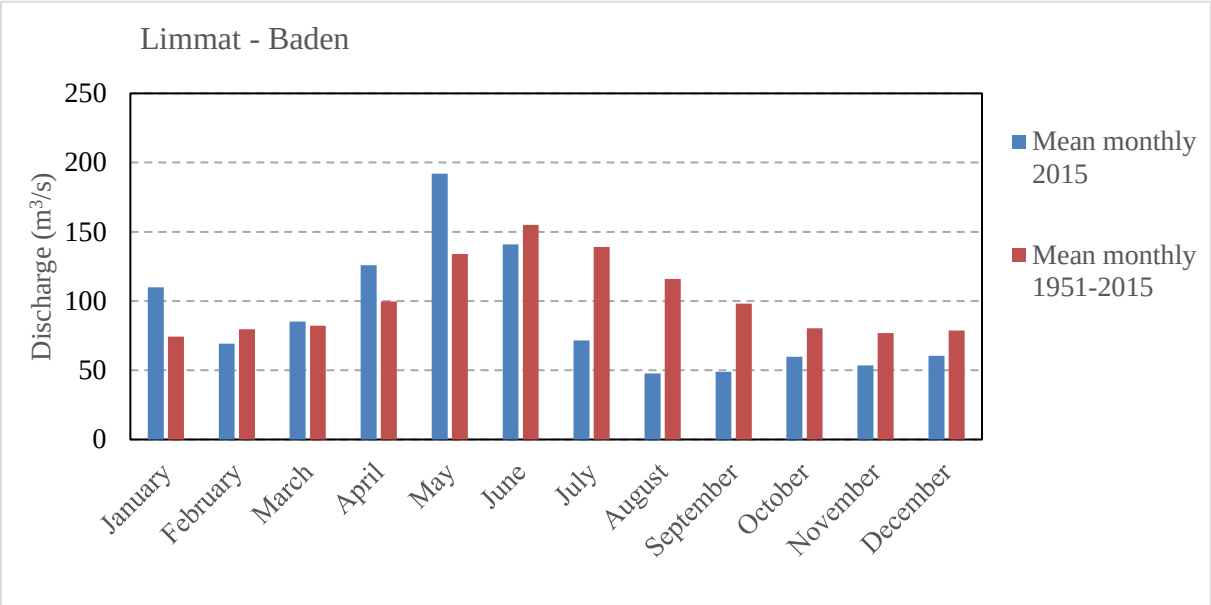

Figure 2: Mean monthly discharge of river Limmat at Baden (AG) (source: https://www.hydrodaten.admin.ch)

1.1.2 Main pressures

River Limmat is located in the river Rhine catchment, which was historically one of the most important Atlantic salmon rivers in Europe. The upstream migration of salmons (*Salmo Salar*) in the Rhine catchment became almost impossible due to transverse structures such as hydropower plants. In the past few years most of the HPPs at the river Limmat have been equipped with state-of-the-art fish upstream passage facilities. However, downstream migration measures and sediment management strategies are not entirely realized at each HPP in river Limmat. The following domestic species face potential mortality during downstream migration, or difficulties during upstream migration in the Limmat catchment. All of the occurring fish species (at least 22 species) in the river Limmat are facing potential mortality during the downstream migration. Some of the most important species are:

- Eel (*Anguilla anguilla*)
- Brown trout
- Common barbel (*Barbus Barbus*)
- Grayling
- Spirlin
- Nase
- Chub
- Bleak

Furthermore, river Limmat is highly influenced by HPPs and densely populated areas and considered as a heavily modified water body. The river has a moderate ecological potential. Various measures for sediment continuity, fish migration, flow changes, habitat in-channel and morphology off-channel have been implemented in the water body. In particular, an innovative vortex tube for bed load transport

continuity, sediment flushing through weirs and upstream and downstream fish migration facilities have been installed and are in operation at the residual flow HPP Schiffmühle. Mitigation measures in River Basin Managements Plans, which are not yet implemented in the Limmat river, are: fish monitoring, restoration of upstream fish migration facilities along all HPPs in river Limmat and planning and implementation of fish protection and downstream fish migration measures.

1.2 Presentation of the HPP

There are two run-of-river Schiffmühle HPPs on river Limmat in the communities of Untersiggenthal and Turgi near Baden, namely the main powerhouse and the residual flow HPPs. The characteristics of both HPPs are listed in Table 1. Figures 3 and 4 show the locations and close-up photos of the HPPs, respectively. In the scope of FIThydro, the residual flow HPP is the case study HPP and hereafter referred as 'HPP Schiffmühle'.

1.2.1 Location of the HPP

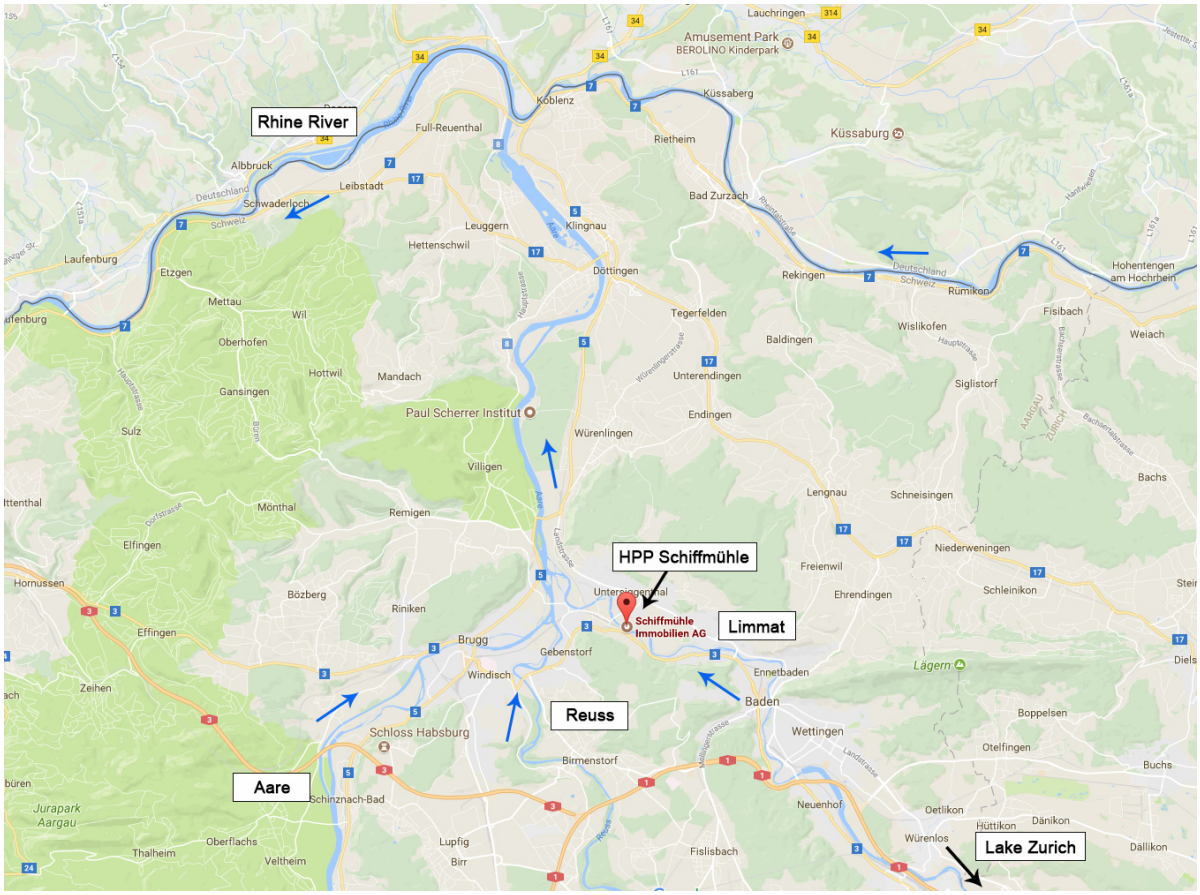

Figure 3: Location of HPP Schiffmühle

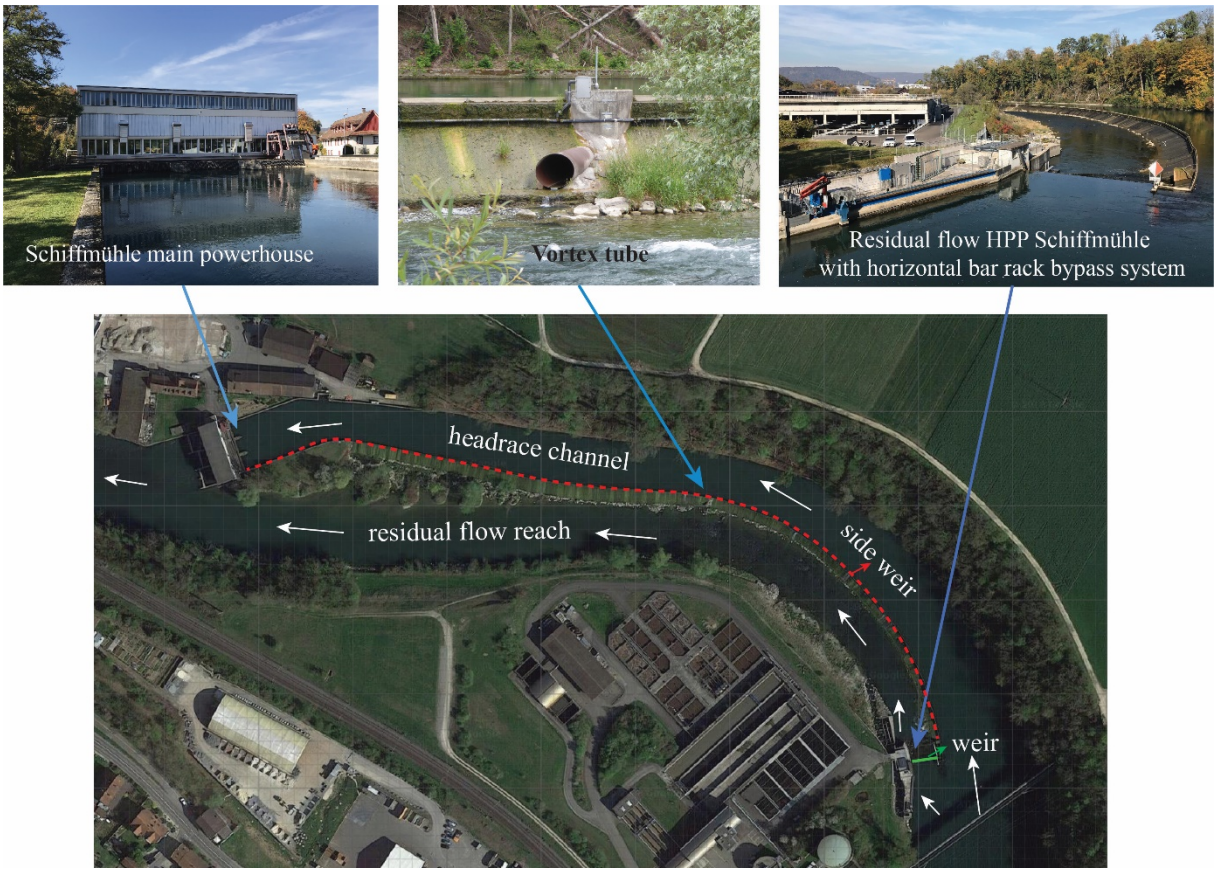

Figure 4: Schiffmühle main powerhouse and residual flow HPPs

Table 1: Main characteristics of the HPPs Schiffmühle

	Schiffmühle main powerhouse	Schiffmühle residual flow HPP
Watercourse	Limmat	
Location :	Untersiggenthal and Turgi near Baden	
Mean annual discharge (1951-2015)	101 m^3/s	
Design discharge	108 m^3/s	14 m^3/s
Head	3.2 m	2.97 m
Capacity	3.46 MW (three vertical Kaplan turbines)	0.50 MW (bevel gear bulb turbine)
Species concerned :	26 fish species known; target species barbel, sprilin, trout, grayling. Salmon expected in the next 10 - 20 years	

1.2.2 E-flow

The HPP Schiffmühle together with an angled fish guidance structure with horizontal bars and a bypass, i.e. a Horizontal Bar Rack Bypass System (HBR-BS) and fish passes provides maximum water of 14.67 m^3/s to the downstream river reach as e-flow. Moreover, during high river discharges, additional water is supplied over the frontal weir at the HPP and over the side weir along the power canal to the residual flow reach (Fig. 4).

1.2.3 Downstream migration devices

At HPP Schiffmühle, a HBR-BS has been implemented in 2013 to protect and guide fish to the downstream of the HPP (Fig. 5). The rack is positioned almost parallel to the main flow to have a lateral intake. The specifications of the HBR-BS are:

- Length of HBR : 14.60 m
- Height of HBR:1.82 m
- Total height of turbine intake: 2.32 m
- Angle of HBR to horizontal: 90°
- Clearance between the bars : 20 mm
- The bars have rectangular profiles/cross section.
- The approach flow velocity at design discharge is 0.5 m/s.
- At the end of the rack there is a bypass with three openings in a vertical chamber at different water depths (close to the bottom, central and close to the water surface).
- 25 cm diameter pipe bypasses fish to the downstream
- Design discharge of the bypass pipe: 170 l/s
- Bypass pipe outlet is about 0.2 m above the tailwater
- 1 PIT-tag antenna has been installed at the bypass to monitor downstream migrating fish

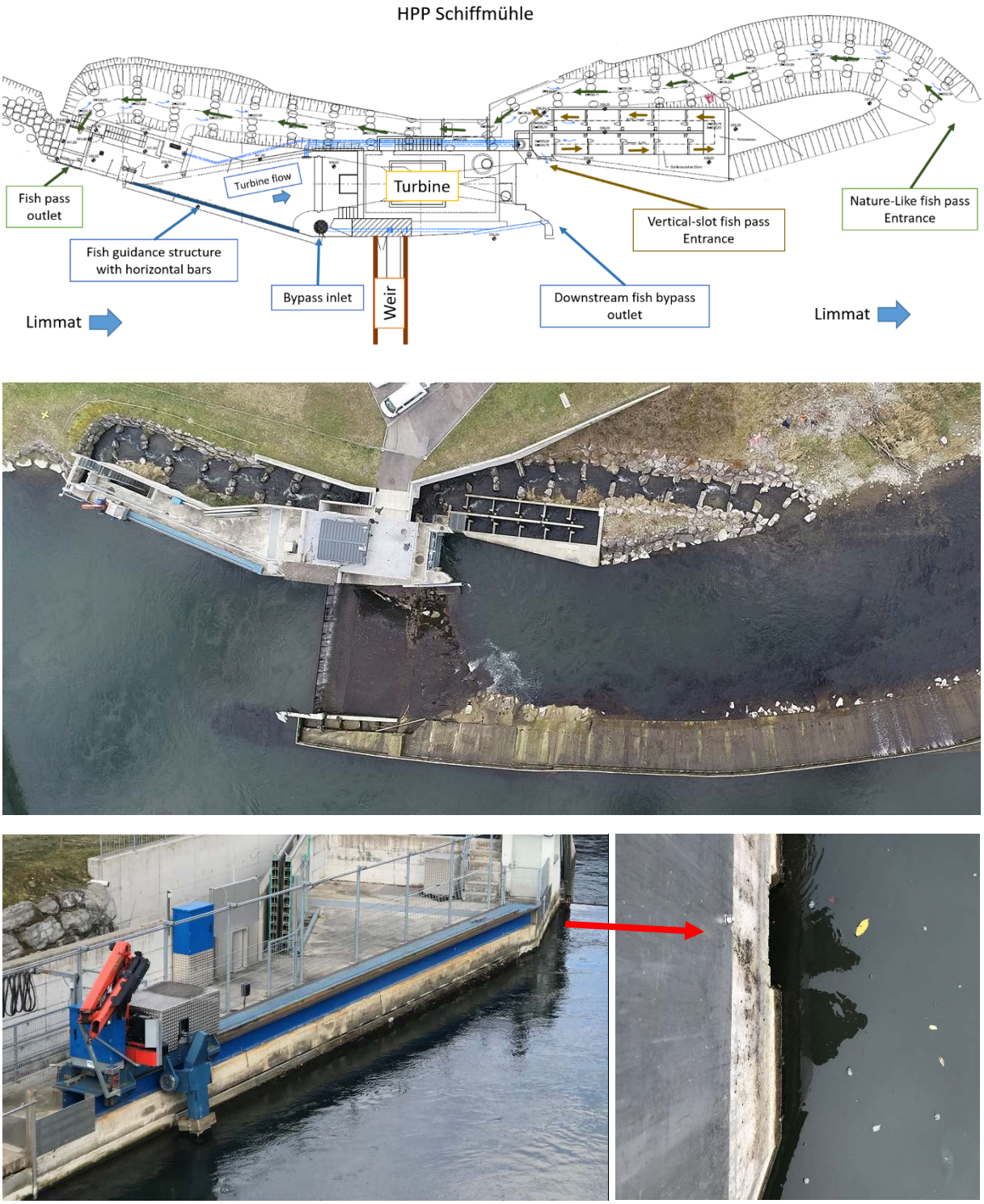

Figure 5: Plan view illustration (top), photo (middle) of HPP Schiffmühle and close-up photo of HBR & bypass inlet (bottom)

1.2.4 Upstream migration devices

HPP Schiffmühle has a combination of a nature-like and a technical fish pass (vertical slot) for upstream migration (Figs. 5 and 6). The specifications of the fishways are:

- The nature-like fish pass entrance is located approx. 36 m downstream of the turbine flow outlet (Figs. 5, 6)
- The bottom slope of the technical fish pass is on average approx. 4 %.
- The technical fish pass entrance is located 2 m downstream of the turbine flow outlet (Figs. 5, 6)
- The bottom slope of the technical fish pass is approx. 6.28%
- The outlet of the technical fish pass is merged to the nature-like fish pass at an elevation of 336.83 m a.s.l.
- Total discharge in both fishways : 0.5 m^3/s
- 5 PIT-tag antennas have been installed in the technical vertical slot fish pass and in the nature-like bypass to monitor upstream migration and fish behaviour in the migration facilities.

Figure 6: Nature-like and vertical-slot fish passes of HPP Schiffmühle

1.2.5 Sediment management

The bedload transport continuity in the Limmat River is strongly impacted by its channelization realized in the 19th century and twelve hydropower plants along its course. The pre-industrial natural bedload transport rate in the reach of HPP Schiffmühle was estimated at 2'000-2'500 m^3/a, whereas today, it is reduced to a few 100 m^3/a, thus the bedload transport can be described as supply-limited. With the execution of multiple bedload restoration measures currently planned along the Limmat River in the context of the Swiss Water Protection Act, the bedload transport rate is estimated to increase again to 1'000-1'100 m^3/a over the next 10 to 15 years (Flussbau AG 2017).

Due to the location of the frontal weir of HPP Schiffmühle in the crossover of a right to a left bend (Figure 1), considerable amounts of bedload are entrained into and deposited along the headwater channel of the power plant (Figure 33). The HPP is thus classified as a significant impairment to bedload transport continuity (Flussbau AG 2017). The accumulated gravel in the headwater channel not only causes the sediment deficit in the downstream reach to further intensify, but also generates operational problems. To maintain the operation of the HPP, the accumulated gravel in the headwater channel has to be extracted regularly. To save extraction costs and restore the bedload continuity, the operator of HPP Schiffmühle installed a vortex tube system to divert bedload from the headwater

channel to the residual flow reach in 2003 (Figure 7) (VAW 2001). The analysis of past gravel extraction records shows that less dredging has been necessary since the installation of the vortex tube. Nevertheless, gravel extraction was necessary in September 2018 and a total volume of 5'300 m^3 was dredged and placed in the residual flow reach (Figure 7). It can be concluded that the vortex tube is diverting a fraction of the entrained gravel to the residual flow reach, but quantitative data on its diversion efficiency is lacking, which is addressed in the scope of the present project.

Figure 7: View of the side weir and the vortex tube at HPP Schiffmühle with the gravel extracted from the headwater channel dumped into the residual flow reach.

2 Objectives of this Test Case

What are we researching?

Downstream fish migration:

The fish guidance efficiency and hydraulics of the HBR-BS are investigated by:

- Fish monitoring using PIT-tagging technique
- Velocity measurements using ADCP
- Numerical modelling of HBR-BS and weir

Downstream impact of sediment management at HPPs:

The dynamic changes in bedload transport rates and total transported masses will be quantified and their effects on river ecology and morphology will be qualitatively evaluated by:

- Monitoring of bedload transport in the vortex tube using an innovative measurement system
- Bathymetry measurements around the HPP using ADCP
- Habitat mapping, sediment sampling, shelter measurements and substrate characterization

Upstream fish migration and habitat modeling:

The effectiveness, attraction flow and potential migration pathways of the nature-like fishway and the technical fish pass (vertical slot) for upstream migration will be investigated, respectively, by:

- Fish monitoring using PIT-tagging technique

- Habitat simulation system (CASiMiR)
- Lateral Line Probe (LLP) measurements

Why do we conduct the above-listed studies at this Test case?

The test case site of HPP Schiffmühle is very practical due to its location near Zurich and is a representative small low-head HPP. The re-licensing of the Schiffmühle main powerhouse in 2011 resulted in an increase in the volume of residual water to be delivered. The HPP owner, Limmatkraftwerke AG, decided to use the environmental water flow by means of a weir turbine for the generation of renewable electrical energy. This led to build the residual flow HPP Schiffmühle with a fish-friendly intake design with a horizontal bar rack and a pipe bypass system. With the construction of the HPP Schiffmühle, the HPP owner replaced the existing fish pass with a new one, consisting of a vertical slot pass and a natural-like fishway. Due to the re-licensing, the HPP owner has started to monitor the effectiveness of fish passes not only at HPP Schiffmuhle but also at his upstream and downstream HPPs, which will provide a good data basis to assess fish migration in that reach of river Limmat. The planned studies at this HPP will address various aspects of fish passes, downstream habitat and sediment transport. The findings of the above listed studies will have a wide range of applications for other similarly sized HPPs and answer the fundamental questions on the fish behavior at fish passes.

What are we expecting?

We expect from this test case (I) to consolidate the design recommendations for fish-friendly water intakes, and technical and nature-like fish passes and (II) to advance in the understanding of the effect of HPP operation including bed load transport via vortex tube on the downstream fish habitat and hydraulics of fish passes on the potential fish migration pathways.

Relevance in FIThydro?

We responded to some objectives of the project and WP2 such as application of the existing SMTDs on a test case, and have had feedbacks on their use and application range (see Deliverable 2.2 of FIThydro, 2019).

3 Presentation and results of activities in FIThydro

3.1 Monitoring of bedload transport through a vortex tube

3.1.1 Data

The negative impact of hydropower plants on the bedload continuity in the Limmat River is of strong interest for the assessment of habitat quality (section 3.4). HPP Schiffmühle is equipped with a vortex tube, a diversion structure for bedload. The vortex tube consists of a steel tube embedded in the side weir, connecting the headwater channel to the residual flow reach (Figure 8). The section of the tube extending into the headwater channel has a slot opening along its soffit and an open end. A gate valve is positioned in the side weir, which is automatically opened when a critical discharge is exceeded. When it is open, a spiral flow develops and bedload transported across the bed of the headwater channel may be entrained into the vortex tube and flushed to the residual flow reach by the combination of the approach flow and the pressure gradient between the headwater channel and the residual flow reach (Mtalo 1988, Atkinson 1994a, Atkinson 1994b, Awasthi 2001). To quantify the diversion efficiency of the vortex tube, three passive acoustic sensors, a geophone, an accelerometer, and a microphone, have been attached to the steel vortex tube (Gray *et al.* 2010). All measurements only concern the sediment transported as bedload, because suspended sediment transport is not an issue.

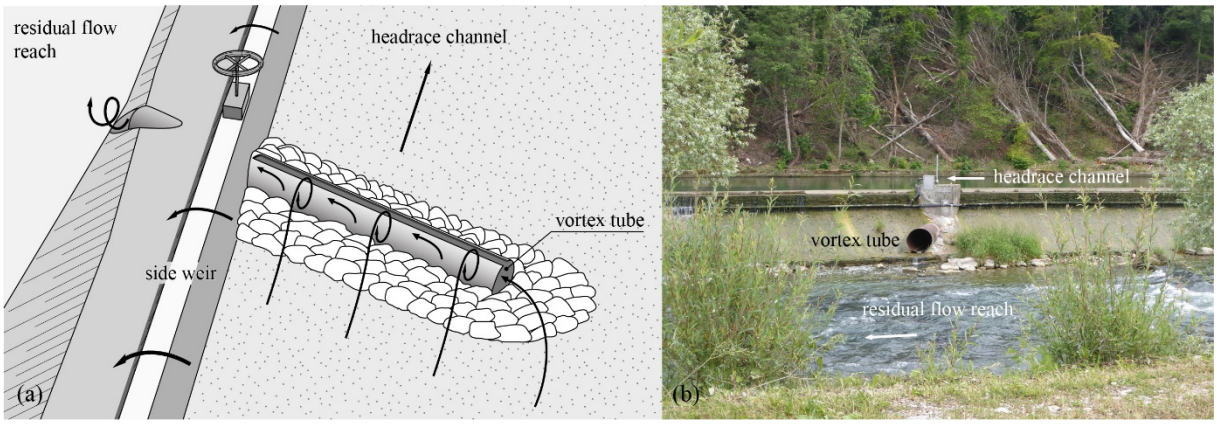

Figure 8: (a) Conceptual sketch of the vortex tube functionality and (b) the vortex tube at HPP Schiffmühle.

The gate valve operation is controlled by the discharge signal of the Swiss Federal Office for the Environment (FOEN) hydrometric station Baden, Limmatpromenade (Station ID 2243), approximately 4800 m upstream of the vortex tube. No major tributaries join the Limmat River in between. The gate valve is opened when the discharge exceeds Q_{open} = 150 m^3/s during the rising limb of a hydrograph and closes when the discharge falls below Q_{close} = 130 m^3/s during the receding limb. Since the beginning of October 2018, the vortex tube is also opened weekly for approximately 22 min, opening and closing time of approx. 5 min included. The goal of the operator is to more regularly divert bedload transported during discharges < Q_{open} into the residual flow reach. To test the functionality of the monitoring system, a test file of 2-4 s length is recorded every day at a set time.

The automatically recorded events up to December 23, 2018 can be sorted into the three main categories (i) flood events (4 events), (ii) weekly flushing (12 events), and (iii) tests (191 events). Figure 9 shows the data set collected until December 23, 2018, including unforeseen operational problems of the HPP or the data recording system. The geophone was installed first in April 2018, later followed by the installation of the accelerometer and the microphone in June 2018. Only the geophone data is thus available for the spring flood events.

Table 2 shows the characteristics of the four spring flood events. Due to difficulties with data storage during the 16-May-18 event, data is only available for 32.3% of its total duration. During the period marked ‘frontal weir out of order’, the discharge allocation to the headwater channel and the residual flow reach was not representative of normal operating conditions. Therefore, the pressure difference between the headwater channel and the residual flow reach may have been influencing the hydraulic conditions and bedload transport in the vortex tube. For this reason, the flood 13-Jun-18 is excluded from the data analysis. Similarly, the first weekly flushing event is excluded due to ongoing gravel extraction works that may have influenced the functioning of the vortex tube.

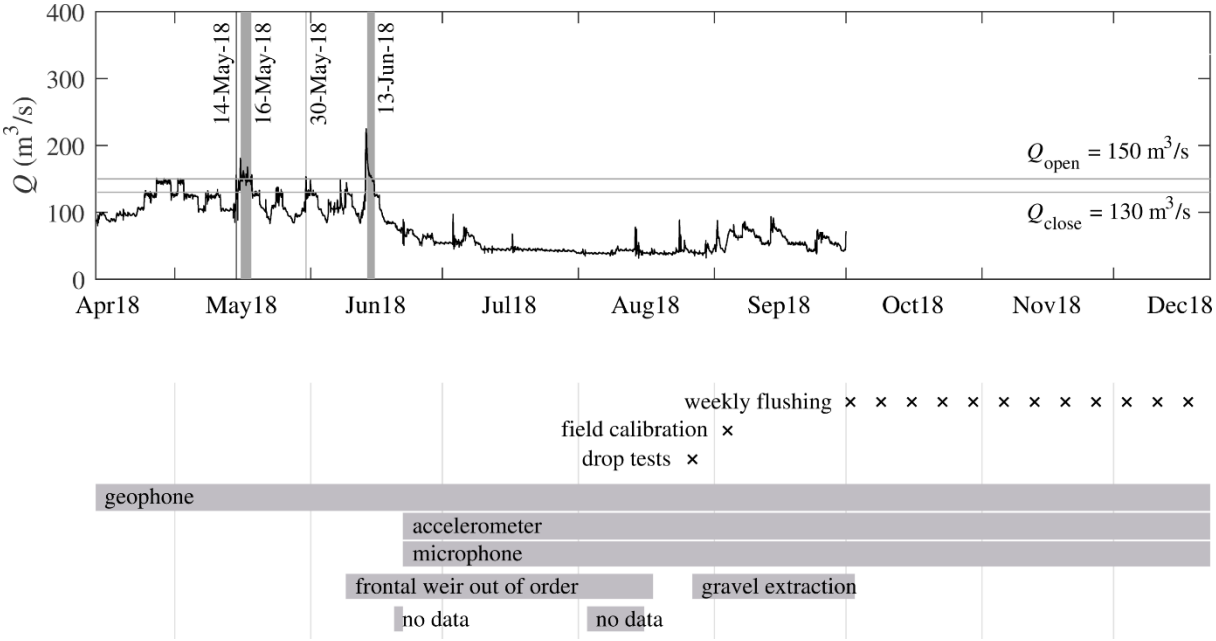

Figure 9: Overview of the data set collected between April 13, 2018 and December 23, 2018. The discharge data (FOEN hydrometric station ID 2243) for October, November, and December 2018 is not yet available. The vortex tube is automatically opened for $Q > Q_{open}$ and closed for $Q < Q_{close}$. Flood events are labeled with their start date. The bottom panel informs about the installation dates of the sensors and restrictions on the data availability due to operational problems of either the HPP or the data recording system. The test events are not displayed individually.

Table 2 : Recorded flood events between April 13, 2018 and December 23, 2018.

Notation	**Start time (UTC)**	**End time (UTC)**	**Duration dd / hh:mm:ss**	**recorded (%)**	**Q_{max} (m^3/s)**
14-May-18	2018/05/14 22:14:00	2018/05/15 01:24:05	-- / 03:10:05	100	155.7
16-May-18	2018/05/16 01:03:40	2018/05/18 09:47:33	02 / 08:43:53	32.3	180.9
30-May-18	2018/05/30 20:35:12	2018/05/30 23:12:16	-- / 02:37:04	100	153.2
13-Jun-18 *	2018/06/13 10:56:24	2018/06/15 12:56:29	02 / 02:00:05	100	224.8

* frontal weir out of order

In this study, we aim to quantify (i) the total bedload mass and (ii) the grain size distribution of the bedload transported through the vortex tube, and (iii) to provide the operator of HPP Schiffmühle with recommendations on the vortex tube operation. A field calibration was performed to relate the obtained signals to bedload transport characteristics (Gray *et al.* 2010). In this report, only the data of the geophone and accelerometer are processed and the analysis is based solely on the signal amplitude. Further data analysis is ongoing.

3.1.2 Methodology

3.1.2.1 Passive acoustic sensors

Three passive acoustic sensors were installed on the vortex tube at HPP Schiffmühle to measure the oscillations of the steel tube caused by grain impacts. A geophone (GS-20DX manufactured by Geospace Technologies, Houston TX, USA), a single axis accelerometer (ICP352C03 manufactured by PCB Piezoelectronics, Depew NY, USA), and a microphone (ICP130A24 manufactured by PCB Piezoelectronics, Depew NY, USA) were mounted in a 0.22 m long, 0.12 m high, and 0.081 m deep, water-tight aluminum housing that was welded to the side of the vortex tube (Figure 10). All signals are recorded by an analog-digital converter with a sampling frequency of f_s = 51.2 kHz. These raw signals are then transmitted and further processed.

Figure 10: The bedload monitoring setup with (a) the housing and the geophone and (b) the housing mounted to the vortex tube and all sensors installed.

Figure 11 shows an exemplary geophone and accelerometer signal with the threshold A_{min} (V) above the background noise level, the maximum amplitude A_{maxmax} (V) and the impulse count *SumIMP* for the period shown. To facilitate data analysis, all recorded raw signals are aggregated in the summary values *IMP*, the sum of the impulse count per second, and A_{max}, the maximum positive amplitude value within a second (Rickenmann *et al.* 2014). The parameters *SumIMP* and A_{maxmax} represent the same summary values, but they are calculated over the duration of an entire event (e.g. a flood).

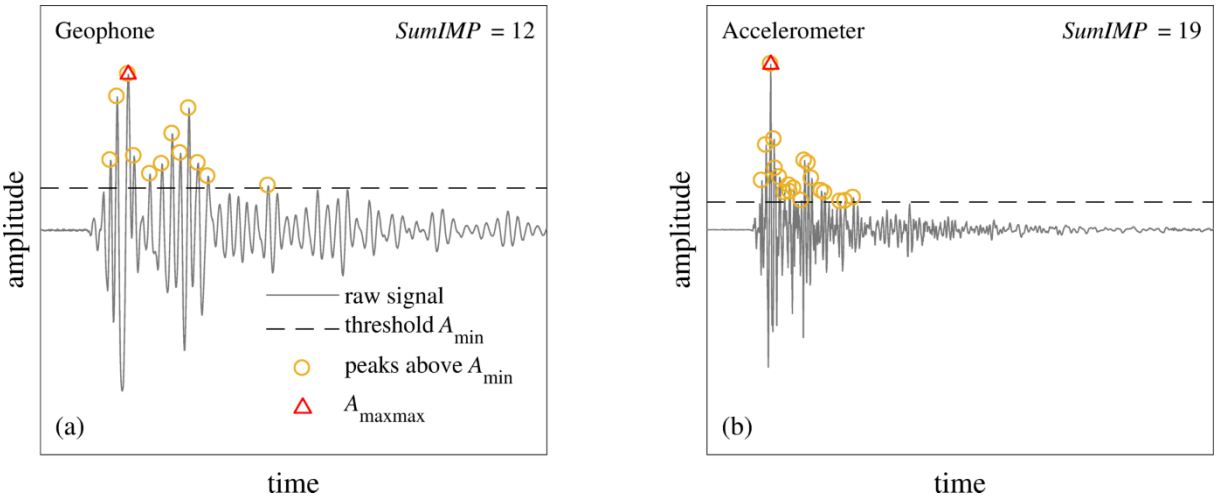

Figure 11: Exemplary (a) geophone and (b) accelerometer signal of the same grain impact. *SumIMP* denotes the total number of peaks above the threshold amplitude A_{min} for the event shown. A_{maxmax} is the maximum amplitude registered during this event. Only positive amplitude values are considered.

3.1.2.2 Pressure sensor

In addition to the bedload monitoring sensors, a pressure sensor (26W manufactured by Keller AG, Winterthur, Switzerland) was installed next to the vortex tube outlet to record water levels in the residual flow reach relative to the vortex tube bottom (Figure 12). The sampling frequency is 1 min^{-1}, independent of the vortex tube operation. The information on the water level at the vortex tube outlet is of interest because the vibration signals may be influenced by submergence of the vortex tube outlet. Additionally, the diversion efficiency of the vortex tube is attenuated by a rising water level at the outlet (VAW 2001, VAW 2017). The pressure sensor data will not, however, be analyzed in this report.

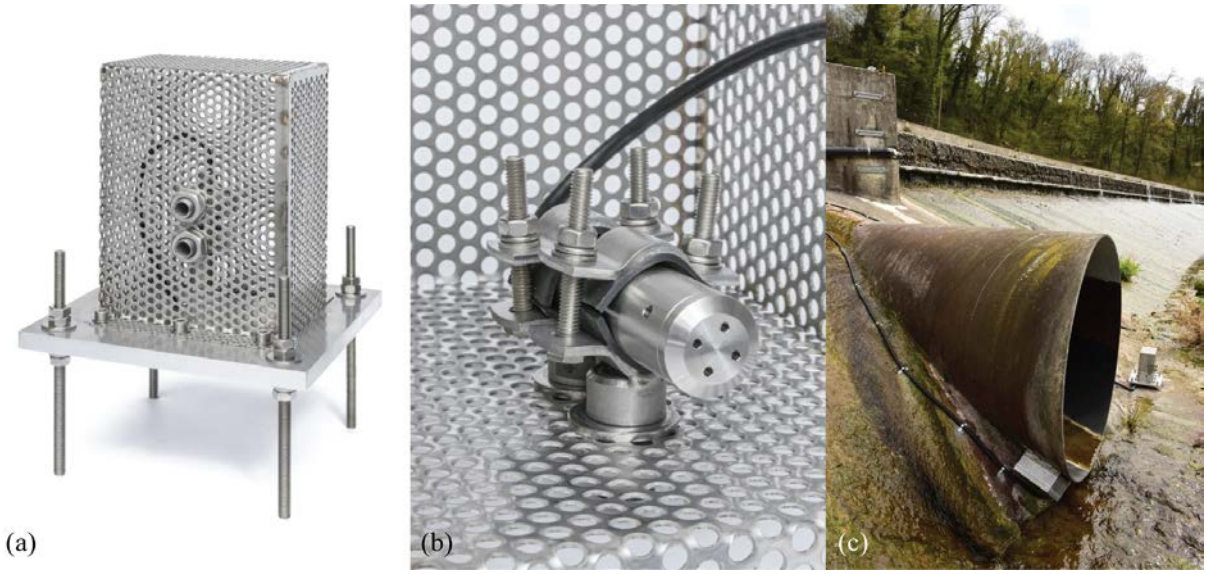

Figure 12: The setup for water level measurements with (a) the housing, (b) the sensor, and (c) the installation next to the vortex tube outlet.

3.1.2.3 Field calibration

On September 4, 2018, the vortex tube was calibrated in the field with four sediment mixtures of known grain size distributions that were flushed through the vortex tube. The grain size distribution analysis of these mixtures was conducted by square-hole sieving and with the grain-detection software BASEGRAIN (Detert and Weitbrecht 2013). The images for BASEGRAIN were taken with a SONY ILCE-6000 and no distortion correction was applied. To obtain the real *b*-axis of the grains, a correction factor of $b_{sieve} / b = 0.80$ (Graham *et al.* 2010) and $b_{BASEGRAIN} / b = 0.85$ (Stähly *et al.* 2017) was applied.

The samples *fine*, *medium*, and *coarse* were obtained from an external gravel extraction site, whereas the sample *channel* is gravel directly excavated from the headwater channel (Figure 7). Table 3 and Figure 13 show the grain size distributions (GSD) and characteristic grain sizes of all sediment mixtures used in the field calibration.

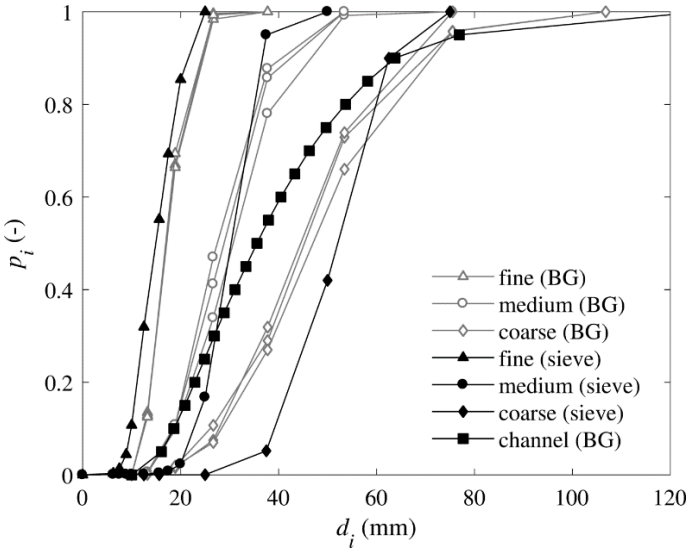

Figure 13: Grain size distribution of the four gravel mixtures used in the field calibration. The legend indicates whether the grain size sample was processed by square-hole sieving (sieve) or by BASEGRAIN analysis (BG).

Table 3: Characteristic grain sizes and the geometric standard deviation $\sigma_g = (d_{84}/d_{16})^{1/2}$ of the sediment mixtures used in the field calibration and in the turbine inlet (BG = BASEGRAIN, sieve = square-hole sieve).

sediment mixture	d_{16} **(mm)**	d_{50} **(mm)**	d_{84} **(mm)**	σ_g **(-)**
fine (sieve)	10.6	14.9	19.8	1.36
medium (sieve)	24.7	30.3	35.7	1.20
coarse (sieve)	41.2	52.1	60.9	1.22
channel (BG)	21.3	35.6	57.3	1.64
turbine inlet (BG)*	16.9	27.2	46.1	1.65

* not used in field calibration

During the field calibration, the vortex tube was opened and closed six times (Table 4). The first opening CW served as calibration of the clear water signal and the flushing of any movable sediment in the vicinity of the vortex tube. During the subsequent calibration runs, the sediment mixtures were dumped in the upstream vicinity of the vortex tube by an excavator set up on a float (Figure 14). The material was dumped with the vortex tube closed and it was opened only afterwards. The river discharge Q was 72.5 m^3/s.

The field calibration is based on the assumption that all of the dumped material was transported through the vortex tube. It is questionable if this assumption holds, as part of the sample may have been entrained by the flow to pass the vortex tube and be transported further along the headwater channel or it may have been deposited and not entrained by the increased flow velocity following the opening of the vortex tube. The relative importance of these processes can be assessed by considering the hydrological conditions. The bed shear stresses during the calibration runs (Q = 72.5 m^3/s) are too small to entrain grains larger than 4-8 mm, as was deduced from ADCP measurements in March 2018 with Q = 62-71 m^3/s (Section 3.3.3.1). Compared to the GSD of the sample mixtures shown in Figure 13, it is therefore unlikely that a large fraction of the sample was by-passing the vortex tube. Moreover, laboratory tests have shown that the opening of the vortex tube strongly influences the local flow field and establishes a suction effect that is especially strong when the water level difference between the headwater channel and the residual flow reach is large (VAW 2017). As a result of the low discharge and therefore large water level difference on the day of the calibration, the relative flow field change caused by the vortex tube was strong and likely entrained most of the dumped gravel.

Nevertheless, there is no way of knowing exactly what fraction of the total bedload volume was passing through the vortex tube and has thus induced impact signals. This uncertainty would have been reduced if the number of calibration runs and the variation in sample volume had been increased or if it had been possible to conduct systematic flume experiments, as it is generally recommended for indirect bedload monitoring systems (Gray *et al.* 2010, Wyss *et al.* 2016b, Wyss *et al.* 2016c). Also, a bedload sampling system downstream of the vortex tube outlet would have been necessary to improve the calibration (compare Rickenmann *et al.* 2012). The simple and relatively inexpensive calibration approach applied here was adjusted to the study purpose.

Table 4: Field calibration runs of September 4, 2018. The duration includes the opening and closing time of the vortex tube. The material was dumped in between the calibration runs, when the vortex tube was closed.

Notation	Sediment mixture	Volume (m^3)	Start time (UTC)	End time (UTC)	Duration (s)
CW	-	-	2018/09/04 08:06:53	2018/09/04 08:18:57	725
CF1	fine	0.5	2018/09/04 08:22:52	2018/09/04 08:34:56	725
CF2	fine	0.5	2018/09/04 08:36:53	2018/09/04 08:48:57	725
CM	medium	1	2018/09/04 08:50:53	2018/09/04 09:08:57	1085
CC	coarse	1	2018/09/04 09:10:53	2018/09/04 09:24:57	845
CCH	channel	approx. 2	2018/09/04 09:28:53	2018/09/04 09:43:57	905

Figure 14: Field calibration on September 4, 2018 with (a) an excavator set up on a float and (b) the outlet of the vortex tube during a calibration run.

3.1.2.4 Data analysis

From the field calibration data, the background noise level was determined to be 0.015 V for the geophone and 0.01 V for the accelerometer. To investigate the influence of the grain size diameter on the vibration signal, the dataset of the field calibration was used to relate the maximum recorded amplitude per event A_{maxmax} (V) to the maximum grain size diameter D_{max} (mm). D_{max} was determined from the square-hole sieve analysis and largest detected particle in the BASEGRAIN analysis (Figure 13). Following Wyss *et al.* (2016a), a power law function of D_{max} is fitted to A_{maxmax} (Figure 15)

$$A_{\max\max} = 2.85 \cdot 10^{-4} \cdot D_{\max}^{1.80} \quad (1a)$$

$$A_{\max\max} = 1.62 \cdot 10^{-3} \cdot D_{\max}^{1.44} \quad (1b)$$

where Eq. (1a) represents the geophone data with an RMSE = 0.11 V and Eq. (1b) the accelerometer data with an RMSE = 0.20 V. This corresponds to the 95% quantile at ± 0.22 V for the geophone data and ± 0.40 V for the accelerometer data, respectively. The smallest detectable grain is 9.0 mm for the

geophone (A_{min} = 0.015 V) and 3.5 mm for the accelerometer (A_{min} = 0.01 V). This relation will be used during future data analysis to extract the GSD of the impulse signals.

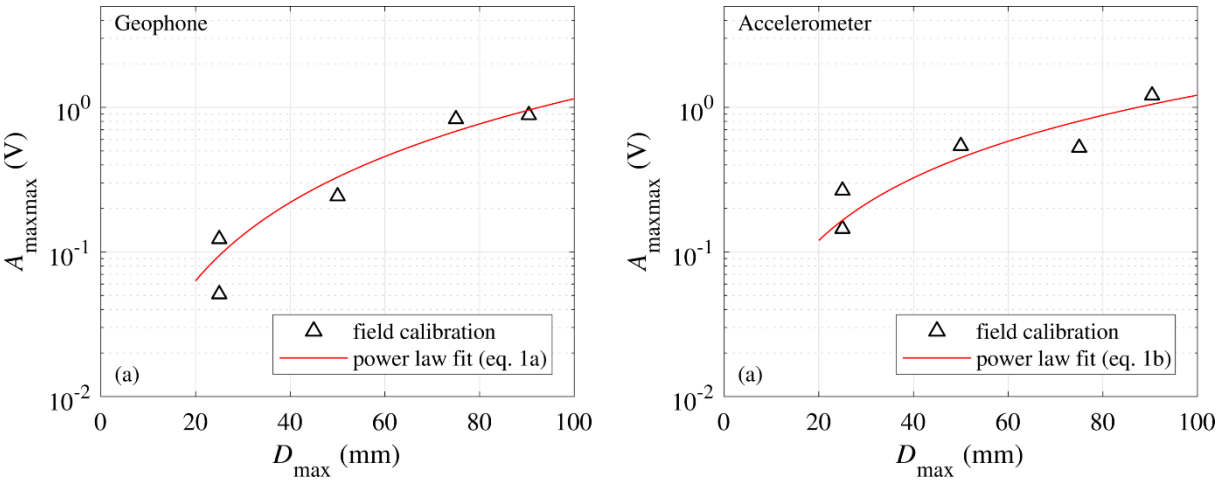

Figure 15: The maximum amplitude A_{maxmax} as a power law function of the maximum transported grain size D_{max} for each field calibration runs.

To extract information about the transported bedload volume from the monitoring system, it is linked to the sum of impulses *SumIMP* above a certain amplitude threshold A_{min}. A linear regression has been shown to be a good model for several impact plate geophone systems (Rickenmann *et al.* 2014)

$$SumIMP = a + b \cdot V_b \tag{2}$$

where *SumIMP* (-) is the total of impulses above a certain threshold A_{min} (V) and V_b (m^3) is the total transported bedload volume during an event. For A_{min}, the background noise level was used. In addition, the sum of the impulse counts and the bedload volumes of CF1, CF2, CM and CC calibration runs (Table 4) were also used as a fifth data point. This is possible when adapting the assumption that the relation between total impulse count and bedload volume is linear (Rickenmann *et al.* 2014). The calibration run CCH was used to validate the model as its bedload volume (Table 4).

Figure 16 shows the best linear regression fit for both datasets with its calibration and validation data points. The parameters of Eq. (2) are a = −484 and b = 10210 m^{-3} for the geophone and a = −781 and b = 7508 m^{-3} for the accelerometer. The model based on the accelerometer data (Figure 16b) seems to be slightly more accurate.

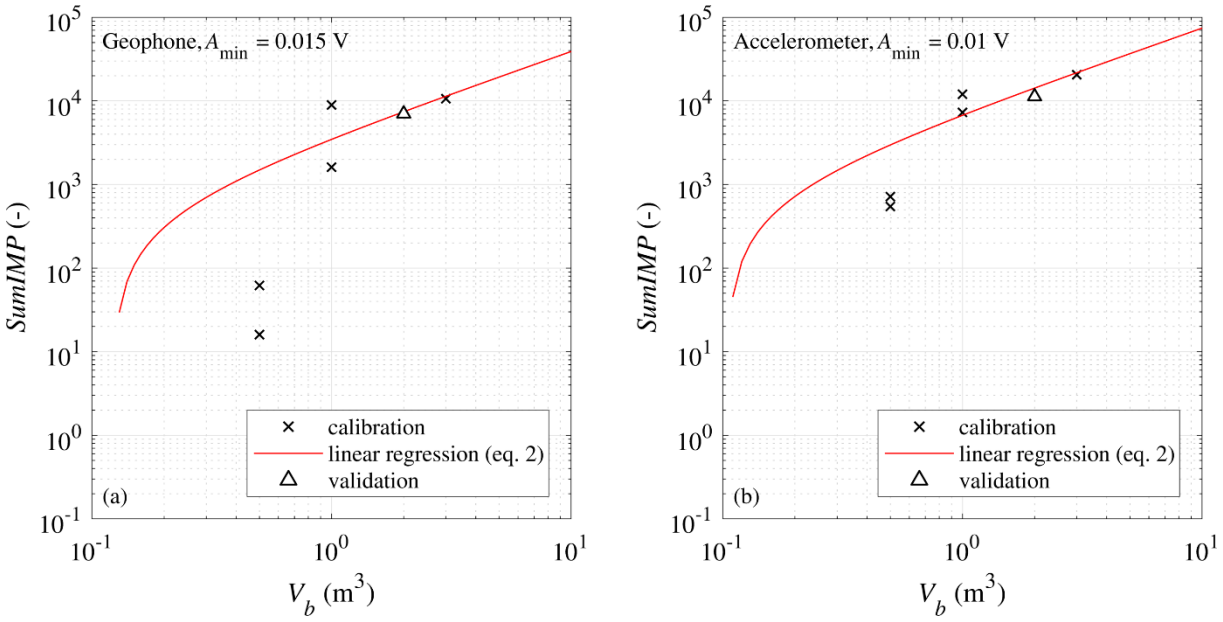

Figure 16: Linear relation between the total transported bedload volume V_b and the sum of impulses *SumIMP* during the field calibration runs for (a) geophone data and (b) accelerometer data.

3.1.3 Results

The transported bedload volumes during eleven weekly flushing events and three spring floods were determined by applying the linear relation to the sum of impulses (Eq. 2). Figure 16 was extended with the results (Figure 17). According to the fit of the geophone data based on A_{min} = 0.015 V, the transported bedload volumes were (i) 0.16 m^3 on May 14, 2018, (ii) 0.27 m^3 on May 16, 2018, and (iii) 0.48 m^3 on May 30, 2018. The accelerometer was not yet installed during these flood events. The transported bedload volume during the weekly flushing events ranged from 0.13 to 0.91 m^3 for the geophone and from 0.10 to 0.33 m^3 for the accelerometer data. The calculated values for bedload transport during the floods and flushing events are thus mostly lower than the volumes dumped during the calibration runs. Some weekly flushing events did not record any impulses on the accelerometer.

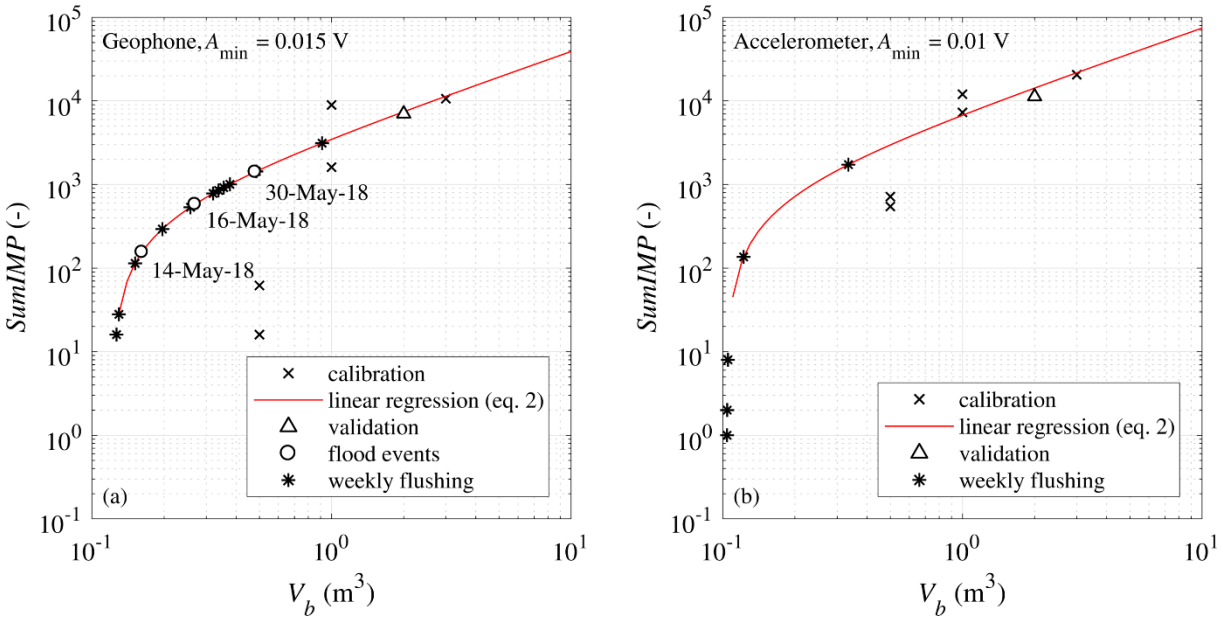

Figure 17: The linear regression between the total transported bedload volume V_b and the sum of impulses *SumIMP* fitted to the calibration runs and the resulting bedload volumes for the flood events and weekly flushings for (a) geophone data and

(b) accelerometer data. Note that the flood events were only recorded by the geophone, as the accelerometer was not yet installed.

The duration of the recorded flood events was either short or they were incompletely recorded (Table 2). It is reasonable that the resulting bedload volumes are relatively small (Figure 17), given that during the calibration runs, material was directly dumped upstream of the vortex tube, while the currently occurring bedload transport in the Limmat River is relatively low. However, with only three flood events recorded so far, it is nearly impossible to assess validity of these results. A record of a prolonged period of vortex tube flushing, i.e. several days, would allow to put the results into perspective. The bedload volumes diverted during the weekly flushing events are in the same range as the flood events, but the data set collected so far is not yet sufficient to make any operational recommendations.

Further insights are expected from the 3D hydro-numerical model that will be set up by AF-Consult (section 3.3.3.4). Bed shear stresses along the headwater channel obtained through the simulation of flood events will enable the estimation of the grain sizes that are transported as bedload. These scenarios will help to assess the quality of the bedload volume determination as well as serve as a validation for future GSD analyses. Furthermore, the ongoing data collection during flood events will eventually allow the connection of the measured bedload transport to the discharge and the comparison to the long-term hydrology and estimates for bedload transport (Flussbau AG 2017).

3.1.4 Conclusions and Outlook

A bedload monitoring system with a geophone, an accelerometer, and a microphone has been installed on a vortex tube, a bedload diversion system at HPP Schiffmühle. It was calibrated in the field by repeatedly dumping sediment samples of known grain size distribution and volume upstream of the vortex tube and subsequently flushing them to the residual flow reach. The results allowed to relate the transported bedload volumes to the impact signals of the geophone and accelerometer. During the flood events and weekly flushing events recorded so far, bedload volumes of < 1 m^3 were determined. These results seem reasonable, but a reliable assessment of their validity is only possible once a larger number of events will be recorded. The amplitude has been shown to also contain information on the transported grain size fractions, however, the quantitative analysis thereof is pending. Additional information on the grain size distribution will be extracted from the frequency spectrum of the impact signals. It can be concluded that the usage of the steel vortex tube as conveyance body and impact plate for passive acoustic bedload monitoring is possible. The first results are promising, but the data analysis will be refined and extended. Furthermore, a larger number of flushing events has to be recorded.

In this report, data collected until December 23, 2018 was processed. The measurement system will continue to record flood events and the analysis of transported total bedload and its grain size distribution will be updated in further dissemination documents. The following steps will be taken during the remaining duration of the FIThydro research project:

- The appropriateness of the correction factors $b_{sieve} / b = 0.80$ (Graham *et al.* 2010) and $b_{BASEGRAIN} / b = 0.85$ (Stähly *et al.* 2017) will be tested by manual measurement of the *b*-axis of all volume sample grains and of all grains being detected on images analyzed with BASEGRAIN.
- A relation between particle size and weight will be established for the bedload at HPP Schiffmühle and the calibration samples from the gravel plant (Bunte and Abt, 2001).

- Parameters influencing the signals, e.g. the grain size, the drop location, or the drop height, will be thoroughly examined by the analysis of several in-situ drop tests that were already performed.
- The probability of signal overlapping will be assessed with the approach of Wyss *et al.* (2016a).
- The analysis of the grain size distribution of the transported bedload will first be completed with the signal amplitude approach (Wyss *et al.* 2016a) and later extended to include the frequency spectra (Wyss *et al.* 2016b, Wyss *et al.* 2016c)
- The microphone data will be analyzed.
- All recorded flood and weekly flushing events will be analyzed.

3.2 Downstream impact of sediment management at HPPs (NTNU, ETHZ)

The dynamic changes in bedload transport rates and total transported masses will be quantified and their effects on river ecology and morphology will be qualitatively and numerically evaluated.

3.2.1 Data

Data will be collected from the field campaign and literature. The information on the sediment structure is collected using different techniques as sieving, pebble count and picture based information based on the evaluation software BASEGRAIN, developed at VAW, ETH Zurich (Detert & Weitbrecht, 2013) Further information about the shelter availability are collected following the Finstad method and the redox potential is measured for potential habitats to get information about the interstitial in this area.

3.2.2 Methodology

- Bathymetry measurements around HPP (section 3.3)
- Habitat mapping, sediment sampling, shelter measurements and substrate characterization

3.2.3 Results

Habitat mapping, sediment sampling, shelter measurements and substrate characterization

For habitat mapping and sediment sampling in the residual flow reach three different well established techniques are used, such as collecting and sieving of the sediment material, picture based sediment distribution evaluation (Buscombe et al 2010) with the program BASEGRAIN and the pebble count method (Bunte at al. 2004). The results will be compared throughout the whole project period and will be used to evaluate the substrate based shelter evaluation. The results described in this report are based on the first field trip in March 2018.

The spots in which the samples are taken represent a broad variety of potential habitats for the relevant fish species in the area (Figure 18). The techniques used for each spot might differ based on the applicability at each location (Table 5). For instance, depending on the water depth and turbidity, it is not possible to use BASEGRAIN in submerged areas as the quality of the pictures is not sufficient. The results are used to compare the different measurement techniques but also to gain information about the structural changes over time in the residual flow reach using further samples which were and

will be taken. These results will be linked with the data gathered in the numerical simulations conducted by the FIThydro partner AF Consult to be able to evaluate the development of the sediment structure as a result of flow changes.

Figure 18: Locations of the sediment sampling in March 2018

Table 5: List of the different methods applied at the testing spots

Data Point	Basegrain	Sieving	Pebble Count
#1	x	x	x
#2		x	x
#3		x	
#4			x
#5	x	x	x
#6		x	x
#7			
#8		x	x
#9			
#10			
#11	x	x	x
#12	x	x	x
#13		x	x
#14	x	x	x
#15	x		x
#16			x

All the three different techniques show advantages and disadvantages as a results of the circumstances of the sampling such as submerged spots vs. non-submerged spots etc. This can be seen in Figure 19 where smaller fractions are underrepresented in comparison with the other two methods. A reason might be that collecting / sieving is an invasive method and the very fine fractions might get lost during sampling. A more detailed evaluation will be available after the evaluation of the other field campaigns.

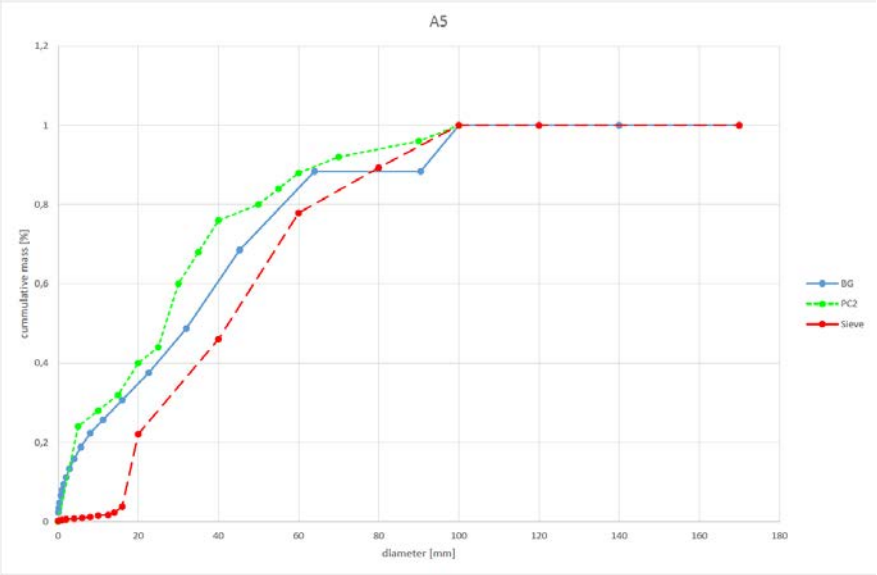

Figure 19: Results of sieving (red dashed), pebble count (green dotted) and BASEGRAIN (blue line) at spot number 5.

The shelter availability is investigated with the method of Finstad (Finstad et al., 2007, Figure 20). The original method shall be adapted to the endemic species in the river Limmat within FIThydro. The availability and the size of the opening in the interstitial are measured with a plastic tube with respect to diameter and depth of the openings. The results are structured in different categories based on the depth S1: 2-5 cm, S2: 5-10 cm, and S3: >10 cm according to Forseth et al. (2014).

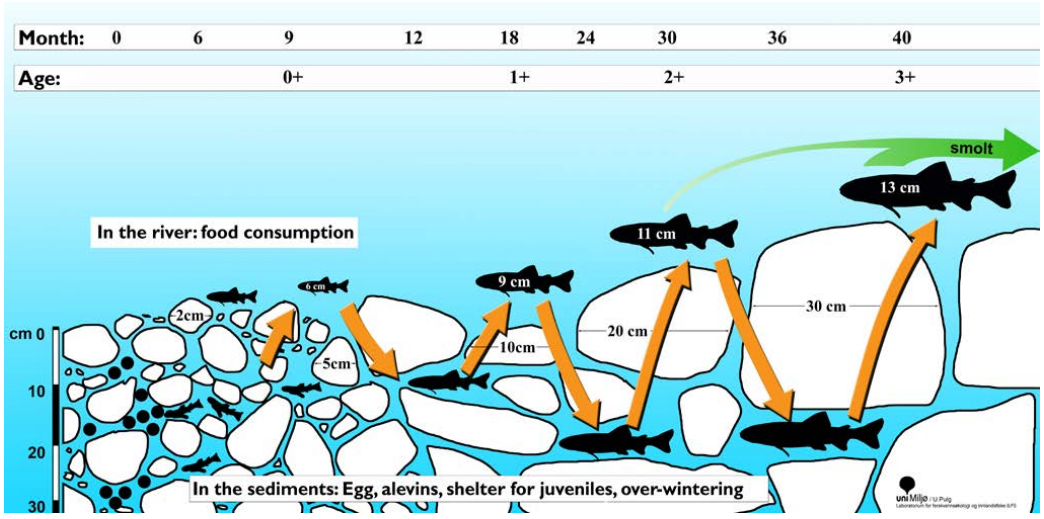

Figure 20: Shelter needs and availabilities depending on the different body sizes of salmons for different ages (Forseth et al., 2014)

Then a weighted shelter availability (Forseth et al., 2014) is calculated:

S1 + S2 x 2 + S3 x 3

and assigned to a class: "low shelter" (< 5), "moderate shelter" (5-10) or "high shelter" (> 10).

The results will be also linked to the grain size distribution. In the river Limmat the sediment percentiles D5 and D10 are much smaller than the ones the method was developed for in Norwegian rivers, therefore also other percentiles and distribution parameters will be evaluated and fitted with the results of the field campaigns.

3.2.4 Conclusion & Outlook

First results are promising. Last measurements were conducted in November 2019 and data analysis is on-going.

3.3 Efficiency of downstream and upstream migration devices (ETHZ, FCO, LKW, AF-CONSULT)

At **HPP Schiffmühle** Horizontal Bar Rack-Bypass System (HBR-BS) has been implemented regarding downstream fish migration. The current situation is documented through field monitoring and 3D numerical modelling in the area near the HBR and the frontal weir. The monitoring comprises the characterization of the flow field and bathymetry using an Acoustic Doppler Current Profiler (ADCP) and a survey of the fish movements. The latter is made with the PIT-tagging technique.

The detailed hydraulic data on the HBR will be obtained from the laboratory investigation in WP3, Task 3.5, and will serve as a basis for the implementation of the HBR into the numerical model. The flow field around the HBR-BS, head losses and upstream and downstream flow fields at HPP Schiffmühle have been simulated using the 3D numerical model. The results from the simulation were compared to the measured values to assess the performance of the numerical model and to deduce potential paths for improvement. Furthermore, fish movements and fish guidance efficiency of the implemented HBR and fish ladders were quantified by PIT-tagging technique (FCO). An antenna mounted in the bypass and fish ladders confirmed the fish passage. Similar fish monitoring campaigns were carried out in two other HPPs upstream and downstream of HPP Schiffmühle on the river Limmat and the obtained data were shared by the operator Limmatkraftwerke. Finally, a comprehensive data set is compiled to study the fish movements on a larger scale. Hydraulics and fish data are evaluated to assess the fish guidance efficiency (FGE) of the HBR-BS and fish ladders. Further investigation in numerically conducted to improve the HBR-BS geometry for better FGE and data analysis is on-going.

3.3.1 Data

Data are collected from the field campaigns, the HPP operator and literature.

3.3.2 Methodology

- Velocity and bathymetry measurements using ADCP and Drone
- Numerical modelling of HBR and weir flow
- Fish monitoring using PIT-tagging technique

3.3.2.1 Hydraulics and bathymetry measurements (ADCP)

Acoustic Doppler Current Profiler (ADCP)

High resolution 3D velocity as well as bathymetry measurements were conducted using an Acoustic Doppler Current Profiler (ADCP) mounted on a remote control boat in March and October 2018. The models of the ADCP and the boat are River Pro 1200 kHz including piston style four-beam transducer with a 5th, independent 600 kHz vertical beam and Q-Boat supplied by Teledyne Marine, USA, respectively (Fig. 21).

The first campaign took place during an average river discharge of Q = 70 m^3/s from 13-15 March 2018, while the second campaign was done on 31st October and 1st November 2018 with an average river discharge of Q = 45 m^3/s. The main goals of both campaigns were to map river bathymetry and measure flow velocities in the upstream and downstream river reaches of the HPP. The data are used to construct, calibrate and validate the 3D numerical model, study the hydraulics of the HBR at the HPP and quantify sediment erosion and deposition in the river. The post-processing was done according to the workflow sketched in Figure 22 using the software WinRiver II[1] and VMT[2]. In addition to the ADCP measurements, we measured flow velocities inside the downstream bypass inlet using a propeller type handheld probe.

Figure 21: ADCP and Q-boat

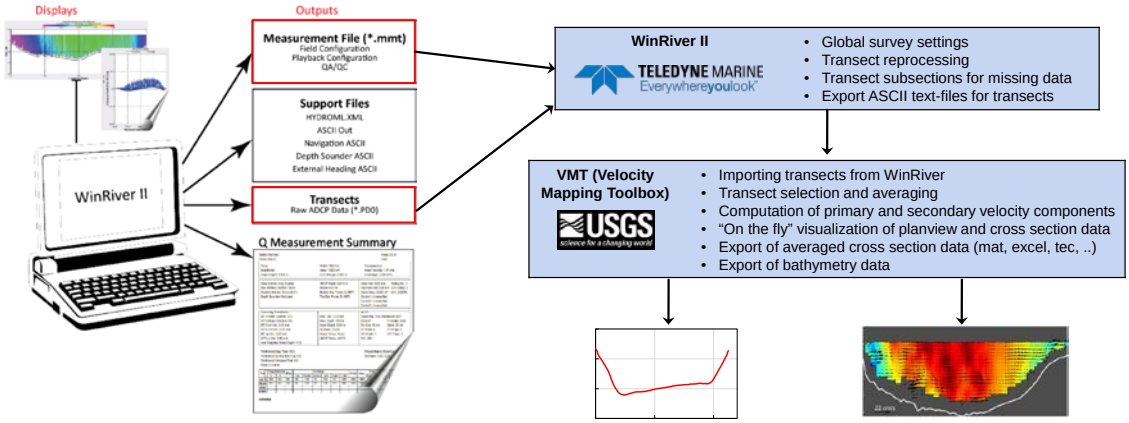

Figure 22: ADCP data analysis workflow

[1] Data collection and post processing software provided by U.S. Geological Survey
[2] Matlab based software for processing and visualizing ADCP data provided by U.S. Geological Survey

ADCP measurement cross-sections at the first (46 cross-sections) and second field campaigns (69 cross-sections) are shown in Figures 23 and 24. Due to a low accuracy of altitude measurement with the DGPS system of the ADCP, we used a TS02 Leica total station and a target on the boat to determine the water surface elevation at each transect during the second field campaign (Figure 25).

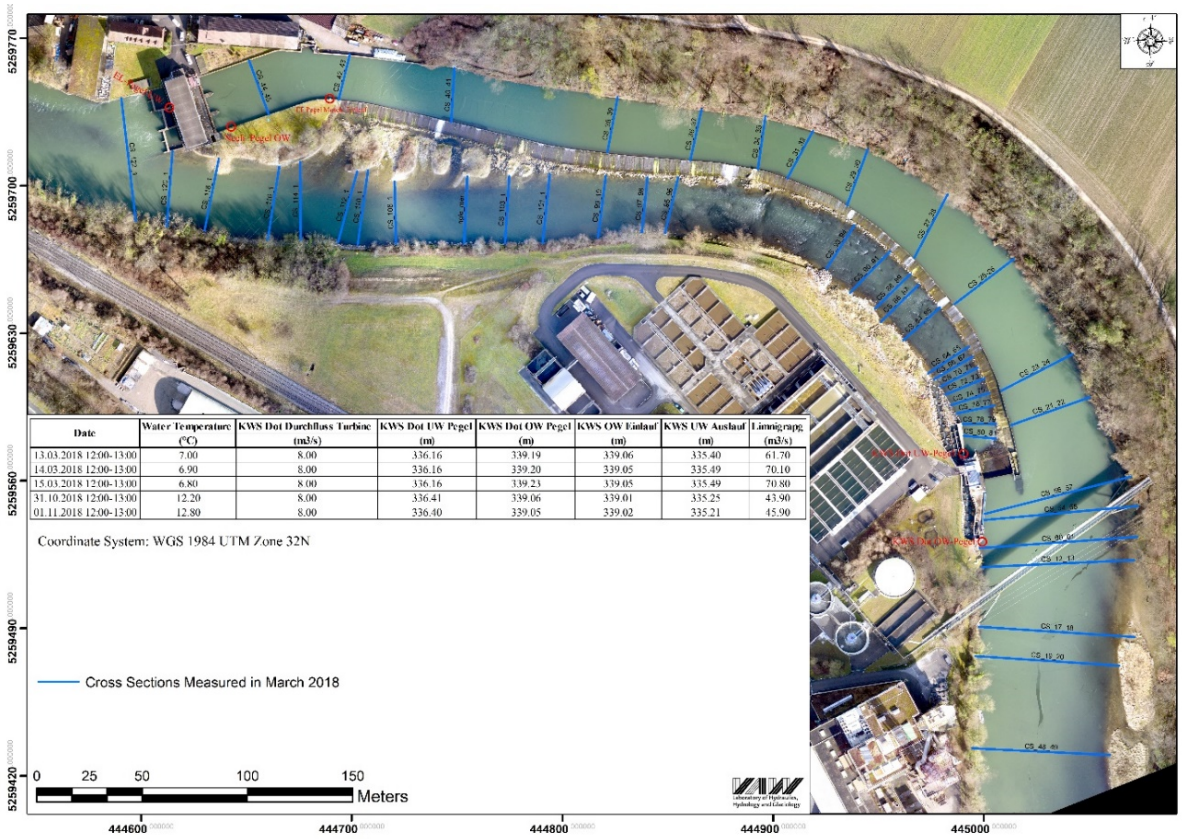

Date	Water Temperature (°C)	KWS Dot Durchfluss Turbine (m3/s)	KWS Dot UW Pegel (m)	KWS Dot OW Pegel (m)	KWS OW Einlauf (m)	KWS UW Auslauf (m)	Limnigraph (m3/s)
13.03.2018 12:00-13:00	7.00	8.00	336.16	339.19	339.06	335.40	61.70
14.03.2018 12:00-13:00	6.90	8.00	336.16	339.20	339.05	335.49	70.10
15.03.2018 12:00-13:00	6.80	8.00	336.16	339.23	339.05	335.49	70.80
31.10.2018 12:00-13:00	12.20	8.00	336.41	339.06	339.01	335.25	43.90
01.11.2018 12:00-13:00	12.80	8.00	336.40	339.05	339.02	335.21	45.90

Figure 23: Velocity and bathymetry measurement locations at HPP Schiffmühle in March 2018

Figure 24: Velocity and bathymetry measurement locations at HPP Schiffmühle in October 2018

Figure 25: Water surface elevation measurements using a total station and a target on the boat

3.3.2.2 Hydraulics (Airborne Image Velocimetry (AIV))

1) Measurement of dry topography

Regionalwerke Baden AG (Zabah, 2018) performed measurements to get a detailed data of the non-wetted topography. To this end, eleven ground control points (GCP) had been measured by geotechnical surveying on 2018/03/08 and a measurement flight had been performed on 2018/03/08 between 10:00-11:00 at a height of 140–145 m over ground. Based on 104 images, a high resolution 3D point cloud had been computed by photogrammetry software *PIX4D*, which combines structure from motion (SfM) technique with MultiView Stereo (MVS) methods. A Digital Surface Model (DSM) as well as an RGB orthoimage each with raster sizes of 0.0244 m had been computed out of it (Figure 26). Georeference is given by the new Swiss survey LV95.

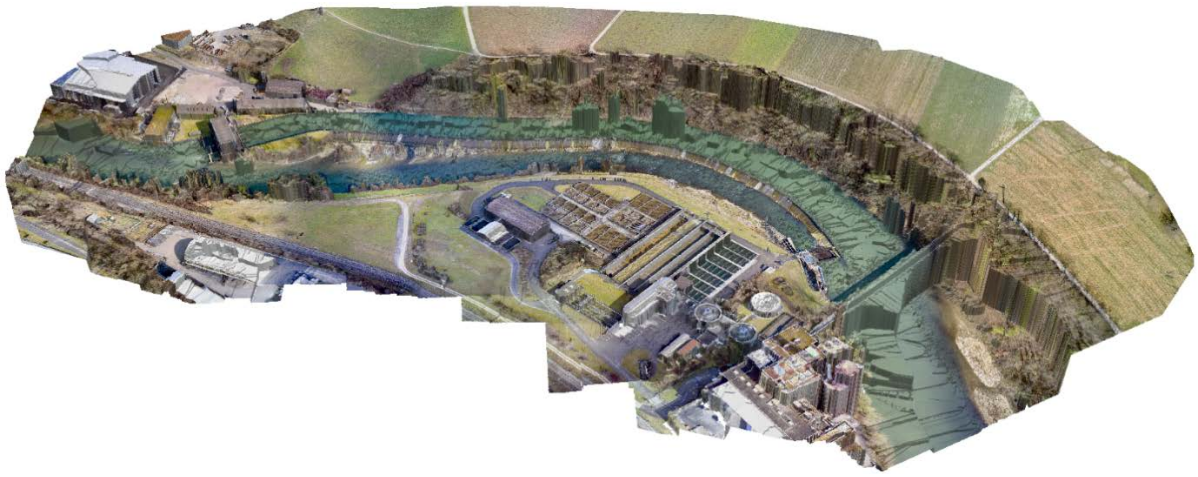

Figure 26: 3D snapshot view to the dry topography area observed by Regionalwerke Baden AG

2) Measurement of surface velocity fields by Airborne Image Velocimetry

Airborne Image Velocimetry (AIV) measurements of surface velocities fields were performed on 2018/03/13 between 11:00-11:45 by VAW/ ETH Zürich (Fig. 27). The flow discharge at this time was almost constant at 71–72 m^3/s, as deduced from the FOEN gauging station Baden-Limmat[3]. The goal of these measurements was to get an overview of the time-averaged far field approach flow.

The AIV technique applied was similar to the one presented by Detert at al. (2017). A crude description of the set-up, performance and image analysis is given in the following, with more information at details deviating from Detert at al. (2017). The AIV measurement setup consisted of an UAV *DJI Phantom 4 Pro+* with a weight of 1.4 kg including a three-axis Gimbal-stabilized action-camera. The latter has a 1” CMOS-sensor and the lens providing a field of view of 84° and a 35 mm focal length equivalent (Figure 27). The total cost of the quadcopter and accessories was below 2 kCHF (March 2018).

Surveying flights were performed at 30–70 m over ground, recording in h.256 video mode at 23.976 fps with a resolution of 4096×2160 px^2. To have a significant grayscale contrast on the video frames the flow was seeded with tracer from the upstream bridge, from a boat and from diverse riparian points during the measurements. Eco foam chips (*FILL-PAC Bio* from *MEDEWO*, Switzerland) were selected with diameters of 30-40 mm (Figure 27).

The total length of the video data set comprises > 20 min, which is too large to be analyzed in total. Therefore, a reduced data set consisting of 579 image pairs each with an internal time shift of $\Delta t_{0:1}$ =

[3] Station #2243, located 4.6–5.1 km upstream, with assumption of an average flow velocity of 1–2 m/s.

5/23.976 s and a median time shift of $\Delta t_{0:1–4:5}$ = 40/23.976 s between the image pairs had been chosen manually for the subsequent image analysis.

Image orthorectification was performed using the photogrammetry software *PhotoScan*, based on the 2×579 = 1158 image frames, combined with the eleven GCPs from Regionalwerke Baden AG (Zabah, 2018) and, to provide more supporting points for the computation, 17 additional characteristic markers as virtual GCPs (e.g. gully holes, larger stones) identified on their dry topography data set.

During the workflow process of *PhotoScan* a frame camera type setting was used to initialize implementation of a camera model that adequately fits the actual lens distortions. The whole process of photograph alignment at original resolution, including computation of camera parameters and positions took about 10 h computational time on a standard PC. The camera positions of the resulting sparse cloud had a reprojection error of ±0.2 px (in image coordinates). *PhotoScan* corrected the 3D coordinates of the GCPs by an average value of ±1.26 m according to the positions measured in the field and gave a reprojection error of ±1.2 px (in image coordinates) for all GCPs. The dense point cloud was reconstructed with medium quality, i.e. the images had been resized by a factor of four, and aggressive depth filtering within 17 h computational time on a typical office PC. The resulting point cloud had a density of 8.1 million points, which is >25 times higher than the density of the sparse cloud. A mesh with 420,000 vertices was build based on 4.5 million manually selected points of the point cloud, i.e. the dense point cloud with misleading points at the water surface and non-riparian points deleted. Finally, 1158 RGB orthoimages with raster sizes of 0.016 m have been exported for the subsequent image velocimetry analysis.

Flow velocities were determined by PIV via the previously described geo-referenced images. The images were converted to 8-bit grayscale, with each individual Gaussfilter-computed background image substracted, and the image intensity was adjusted and pixel values < 40 were capped – as described by the following MATLAB-code lines

```
I = rgb2gray(I);
J = imerode (imbinarize(I,0),strel('square',40));
I = imadjust((I-imgaussfilt(I,10)).*uint8(J));
I(I<40)=0;
```

Then, the MATLAB-based open source software *PIVlab* by Thielicke and Stamhuis (2014) was used to determine the surface flow velocities. PIV analysis was performed to the 579 image pairs in mode [(0,1), (4,5), (8,9), . . .] on a final window size of 64×64 px^2 with 50% overlap. Postprocessing comprised masking out non-water surface areas and applying a universal outlier detection method (Westerweel & Scarano, 2005) to the instantaneous velocity fields to eliminate misleading velocity vectors. The median value of the time series at each grid point was chosen to describe a characteristic time averaged surface velocity. Due to inhomogeneous flow-seeding conditions and non-perfect image orthorectification results (shivering between image pairs) the chosen approach is prone to overestimate near-zero flow velocities. Therefore, velocities <0.2 m/s finally have been deleted.

Figure 27: DJI Phantom 4 Pro and Ecofoam as seeding particles

3.3.2.3 Fish monitoring

Fish were monitored at HBR-BS and both technical and nature-like fish passes using the PIT-tagging technique between 2017 and 2019 (Figs. 28 and 29).

Two antennas in the nature-like fish pass and another two antennas in the vertical-slot fish pass detect the entrance behavior of fishes. One additional antenna at the exit of the fish pass registers the fish leaving the pass. One antenna has been installed in the downstream bypass to detect downstream migrating fish (Figure 28). All six antennas are connected to readers recording detections at a rate of about 14 scans per second. Data from the readers are remotely downloaded and the function of the readers is controlled from the office.

Figure 28: PIT-Tag antennas (left picture in the nature-like fish pass, right picture in the vertical-slot pass

Fish tagging started in September 2017 and finished in 2019. Overall, more than 3000 fish belonging to 16 species were tagged during 3 years of monitoring and released downstream of the fish ladder. Most of the fish were caught in the counting facilities, except 73 individuals that were electrofished on 26-9-2018 upstream of the hydropower plant and translocated to downstream areas. Smaller fishes (< 160 mm) were tagged with 12 mm PIT tags, larger fishes (> 159 mm) with 32 mm tags. With a small incision the tags were placed in the body cavity. For the handling fishes were anesthetized with clove oil (30 mg/l) (Figure 37). Before releasing fish back to the water they could fully recover from anesthesia.

Figure 29: left: bleak with 12 mm PIT-tag, right: barbel, one of the most abundant species in the Limmat River

3.3.2.4 Hydraulics (Numerical modelling)

Flow conditions upstream and downstream of the HPP are simulated with the software FLOW-3D (Flow Science, 2014). The goal is to simulate flow conditions at the in- and outlets of the fish migration structures at variable Limmat discharges and, accordingly, with variable operating conditions of the hydropower plants. The following modelling concepts are applied.

Horizontal Bar Rack-Bypass System (HRB-BS)

The Horizontal Bar Rack (HBR) is simulated in FLOW-3D by applying a baffle. This allows to account for the hydraulic effects of the rack without having to simulate each individual bar by direct numerical simulation with a resolution fine enough to properly resolve its hydraulic effects – an almost impossible endeavour given the rack size and bar spacing. It has been shown by specific research (Krzyzagorski, 2016), that the representation of a trash rack by a baffle leads to correct hydraulic effects.

Since the rack is not aligned with the orthogonal model cells, FLOW-3D fits the rack in a stepped shape on the grid. This artificially increases the rack surface. By reducing the porosity of the rack, the increase can be compensated as follows:

$$\phi_{model} = \sin(\alpha) \cdot \phi_{rack}$$

where:

ϕ_{model} Porosity to be entered into model

ϕ_{rack} Porosity of the rack

α Angle between grid and rack (0 = aligned)

With this correction, the open surface of the rack and therewith the flow velocities within the rack are properly represented.

The horizontal direction of the approach flow is not influenced by the rack since the bars are horizontally arranged. The impact on the vertical flow direction is not considered here because of the small vertical velocity component.

The loss coefficient assuming a 5 % obstruction and perpendicular flow is calculated based on the formula developed by Meusburger (2002, pages 170/171).

$$\zeta_{obstruction} = \left(\frac{P}{1-P}\right)^{\frac{3}{2}}$$

where P is the obstructed flow area. With 5 % obstruction the coefficient is 0.012. Oblique flow direction is directly accounted for by the FLOW-3D simulation.

Bypass system of HBR

The bypass of the HBR is designed for a discharge of 170 l/s when the weir flap is fully raised. The inlet of the bypass consists of two rectangular openings at different depth in the side wall of the HPP structure approximately 4 m upstream of the weir. The openings lead to a chamber from where a pipe leads to the residual flow river section. In the model this flow is specified by an outflow boundary condition at the top and an inflow boundary condition at the bottom of the pipe.

Turbine

The flow through the turbine has not been simulated. The model ends before the impeller with an outflow rate boundary condition equalling to the turbine flow. The water is returned to the model by an equivalent inflow boundary condition at the end of the suction tube.

Fish passes for upstream migration devices

To limit the computational power of the simulations the flow through the technical fish pass and the near-natural bypass is not explicitly simulated over the entire length of these structures. Only the flow through the lowest pools of each of the structures is simulated, such that the attracting flows in the residual water section are well represented by the model. The discharges are known and set in the model with outflow and inflow boundary conditions.

Model geometry

For generation of the model geometry, two types of data are combined:

1. As-built drawings of the structures of the residual HPP and of the near-natural bypass.
2. Bathymetry data measured in the present project and additional cross sections further upstream and downstream recorded by FOEN in 2013.

From the as-built drawings a 3D geometry of the residual HPP has been established (Figure 30). The bathymetric cross sections used for establishing the geometry of the Limmat river, the headwater channel and the residual flow section are displayed in Figure 31.

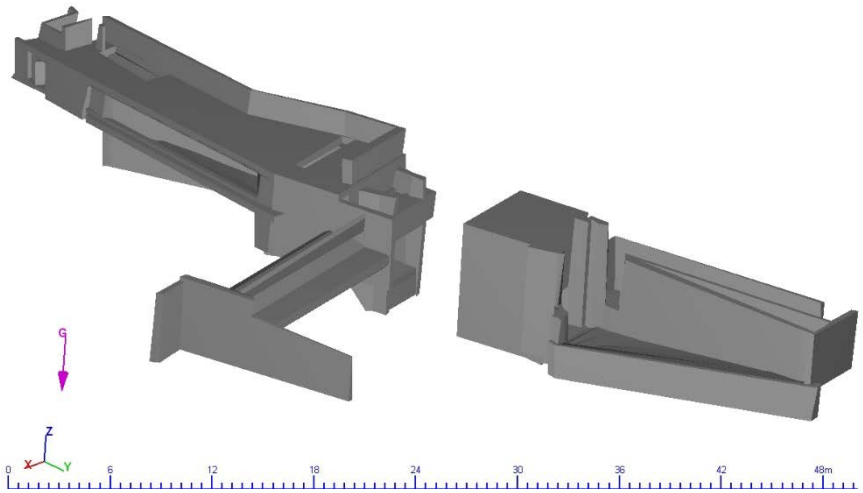

Figure 30: 3D geometry of the residual HPP with upstream (left) and downstream (right) parts

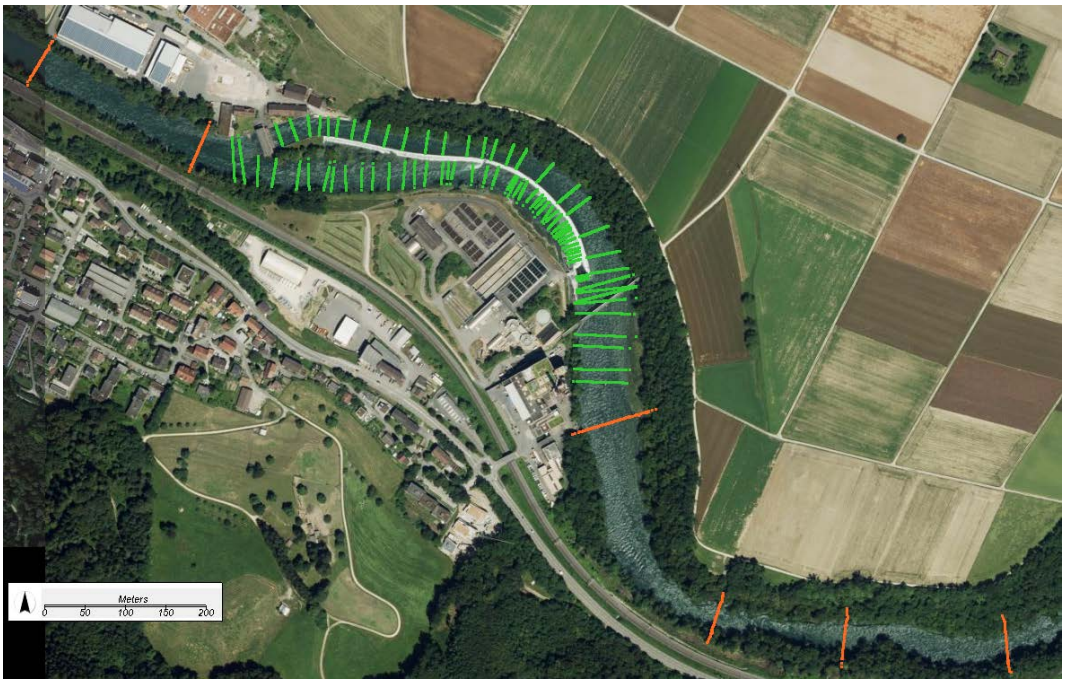

Figure 31: Available bathymetric cross sections, green (this project) and orange (FOEN, 2013)

Boundary conditions

Inner model boundary conditions for individual elements such as the turbine, the fish downstream migration device and the fish upstream migration devices have been described in above sections. The outer model boundary conditions are defined as:

- Inflow boundary condition at the upstream
- Water level to discharge relation at the downstream

Flow condition scenarios

The goal is to simulate flow conditions at the in- and outlets of the fish migration structures at variable Limmat discharges and, accordingly, with variable operating conditions of the hydropower plants.

The Limmat discharge conditions and operating conditions for which the model is to be applied are selected in a two-step approach:

1. Only the periods in which fish migration occurs are considered. These are mid-May to mid-June in springtime and September till beginning of October in fall. In these periods the three residual flow allocations of 8, 10 or 14 m ^{3}/s can occur. As seen in 10, four sub-periods with different prescribed residual flows must be considered.
2. For these four sub-periods, the Limmat hydrograph is analysed and Limmat flows of 5 %, 20 %, 50 % and 95 % are evaluated (Table 6, Figure 32). In total a set of 16 flow conditions are thus considered to be studied as scenarios.

It can be noted that weir overflow, starting at 123 m^3/s, takes places for 6 out of the 16 scenarios.

Table 6: Limmat flow conditions and prescribed residual flows during fish migration periods in spring and fall

Period	Q_{Limmat} 5%	50%	80%	95%	$Q_{residual}$ min.
2nd half of May	295	125	98	68	10
1st half of June	289	136	95	62	14
September	227	91	61	45	10
1st half of October	173	82	57	43	8

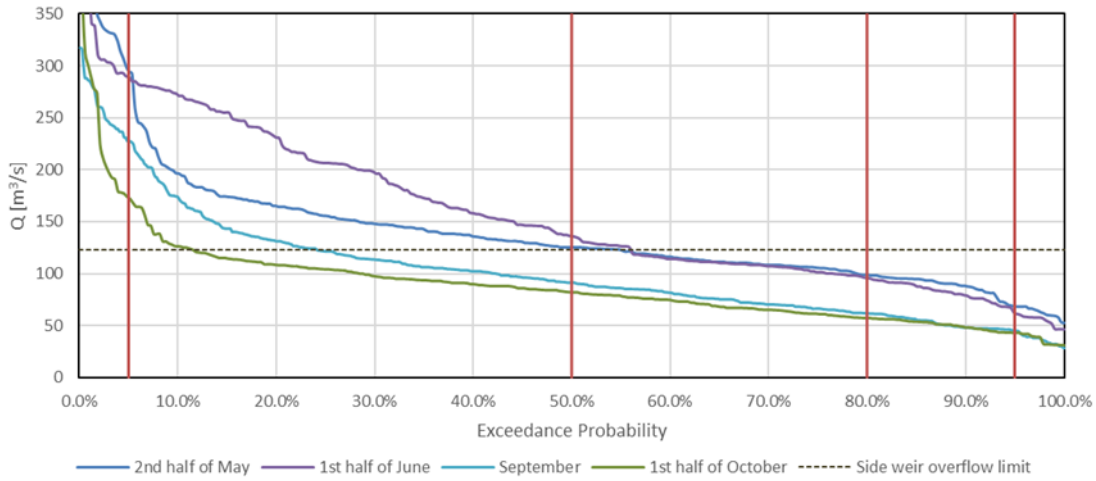

Figure 32: Flow duration curves established based on 1997-2018 Limmat flow data for the four sub-periods of fish migration

Model calibration and validation

River bed roughness values of the model are calibrated in a trial and error approach such as to fit the simulated water levels to the observed ones. Roughness values will be assigned to model sub-areas as shown in Table 7.

Table 7: Calibration of roughness values

Model sub-area	Manning's roughness n [s/m$^{1/3}$]
Upstream & downstream river	TBD
Headwater channel	TBD
Residual flow section	TBD
Concrete structures (overflow weir, headwater channel walls, HPP inlet, vertical-slot fish pass)	TBD
Near-natural fish pass	TBD

Model validation will be against the measured flow velocities and has not yet been conducted.

3.3.3 Results

3.3.3.1 Hydraulics and Bathymetry data (ADCP)

During the field measurements, the discharge in the river Limmat slightly fluctuated around Q = 70 m^3/s and 49 m^3/s in March and October 2018, respectively. The discharge of the residual flow HPP was around 8 m^3/s and total discharge in the residual flow reach was approx. 10 m^3/s including the discharges from the HPP, fish ladder, downstream bypass flow and the side weir along the headwater canal in both field measurements.

Figure 33 show the upstream and downstream river reach bathymetry in March and October 2018. It is clearly seen that the bathymetry in the headwater canal changed and deepened from March to October 2018. This is mainly because of the removal of settled gravels from the headrace channel in September 2018. The removed gravels amounted to approx. 5300 m^3 calculated using the bathymetry maps and were damped into the residual flow reach (Figure 34). Such replenishment of gravels is considered as a measure to improve the downstream fish habitat and to mitigate river bed armouring, bank erosion, channel incision. Major bathymetry and flow depth changes occurred between the vortex tube and the residual flow HPP causing high flow velocities around the fish ladder inlets (Figure 35). We expect that after several flood events, the damped gravels will be transported further downstream of the main HPP and the bathymetry of the residual flow reach will become similar to that in March 2018 with improved habitat quality. Therefore, for 3D numerical model, the bathymetries of the residual flow reach in March 2018 and that of the headrace channel in October 2018 are used.

Figure 35a and b shows the depth-averaged flow velocity distribution in the upstream and downstream flow reaches of the HPP Schiffmühle in March and October 2018, respectively. Note that the river discharges were different but the discharges in the residual flow reach were similar in March and October in 2018. The flow velocity increases from the downstream of the residual flow HPP up to the entrance of the fish ladder and reaches its maximum of 250 cm/s in October 2018 due to bathymetry changes caused by gravel replenishment in September 2018. Downstream of that location, it gradually decreases along the river reach until the downstream of the main powerhouse. In this region, a similar trend is observed in velocity distribution measured in March 2018 (Figure 35a). Although velocity magnitudes are different in March and October 2018, the overall velocity distribution in the headrace channel has changed because of gravel removal in September 2018 compared to that in March 2018.

One of the foci of the present study is to investigate the hydraulics and efficiency of HBR-BS in HPP Schiffmühle. To this end, we conducted densely-spaced ADCP measurements as well as velocity measurement inside the bypass at the HPP. Figure 36 shows the depth-averaged velocity distribution and streamlines around the HPP measured in October 2018. The flow velocities are high just upstream of the HPP close to the left bank of the river. Velocities slightly decrease towards the turbine intake. A discharge of 8 m^3/s goes into the turbine intake and a little flow goes towards the weir and the bypass inlet. The rest of the flow, i.e. about 41 m^3/s, goes into the headrace channel corresponding to about 80% of the river discharge. As indicated with red arrows in Figure 36, most of the fish in the river follow the main stream towards the headrace channel , while a small portion swims towards the HPP. When fish arrive at the HPP, it is likely that they do not find the bypass entrance because of the re-circulation zone and low velocities between the weir and the bypass inlet compared to high flow velocity at the turbine intake (Figures 36 and 37). The design discharge of the bypass is 0.170 m^3/s and the corresponding average velocities in front of the bypass, at two rectangular bypass openings and in the pipe are approx. 0.35 m/s, 2 m/s and 3.46 m/s, respectively (Figure 38). However, the ADCP field data show that the velocity in front of the bypass is around 0.10 m/s instead of 0.35 m/s (Figure 37). To confirm this result, we measured velocities inside the bypass and show the measurement points and velocity data in Figure 38. The average flow velocity at the two rectangular bypass openings is 0.66 m/s and the total bypass discharge amounts to 0.055 m^3/s. For this bypass discharge, the average flow velocity in front of the bypass is 0.11 m/s (Figure 38b), which is in agreement with the ADCP measurement. The measured bypass discharge is less than 1/3 of the design discharge, which is likely due to clogging of the bypass pipe. Although the bypass pipe entrance is regularly cleaned according to the operator, the clogging seems to be unavoidable. Overall, due to mainly the re-circulation zone, low flow velocities in front of the bypass as well as almost zero tangential velocity between the

turbine and bypass intakes, the fish guidance efficiency of the bypass system is expected to be low. We will discuss this result together with the fish monitoring result in the next subsection.

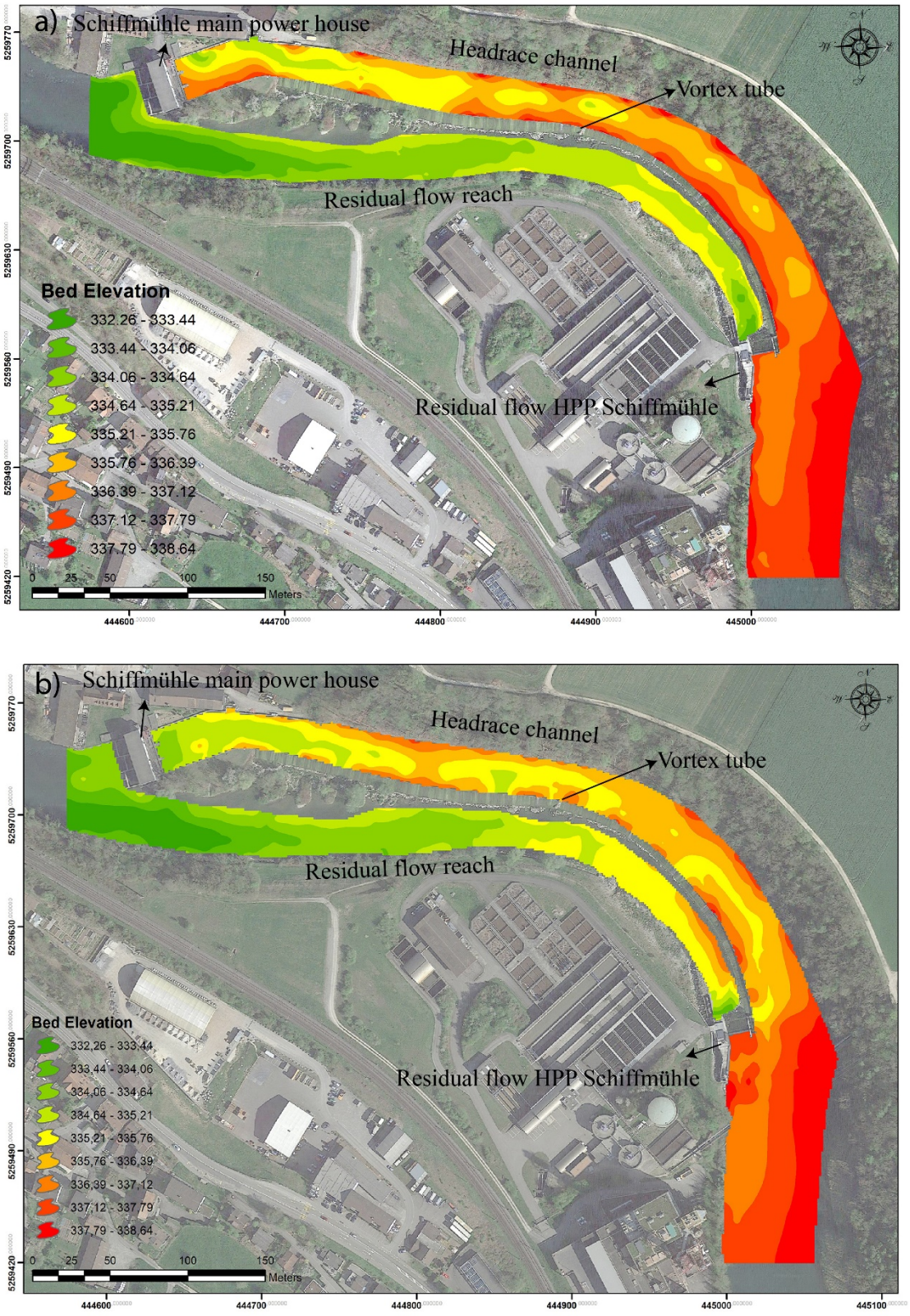

Figure 33: Bathymetry of upstream and downstream flow reaches of the residual flow HPP Schiffmühle in March (a) and October (b) 2018.

Figure 34: Photos of residual flow reach in March (a) and October (b) 2018.

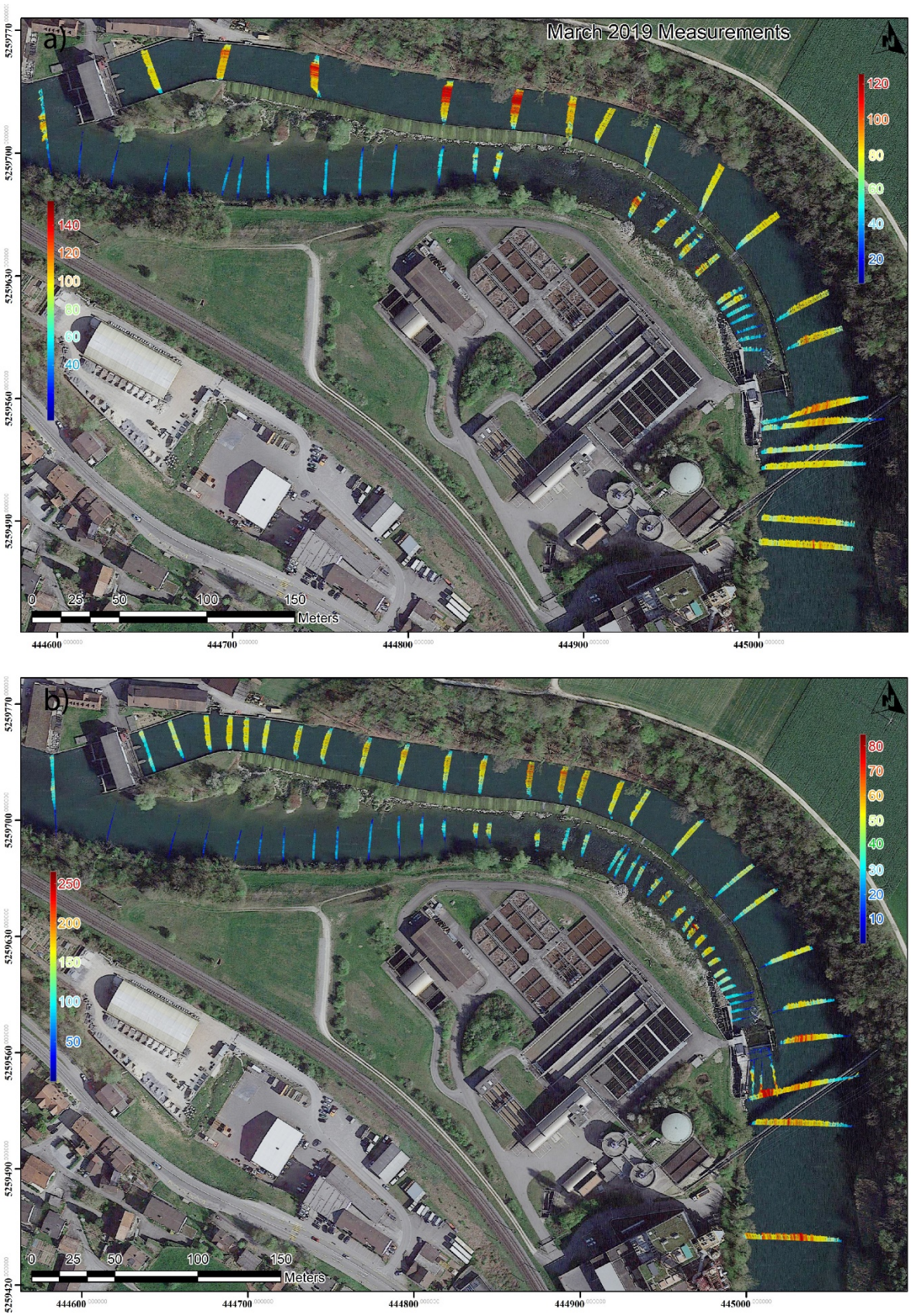

Figure 35: Depth-averaged velocity profiles from ADCP measurements at HPP Schiffmühle in (a) March and (b) October 2018. Note that the left and right colorbars are for the residual flow reach and headrace channel, respectively.

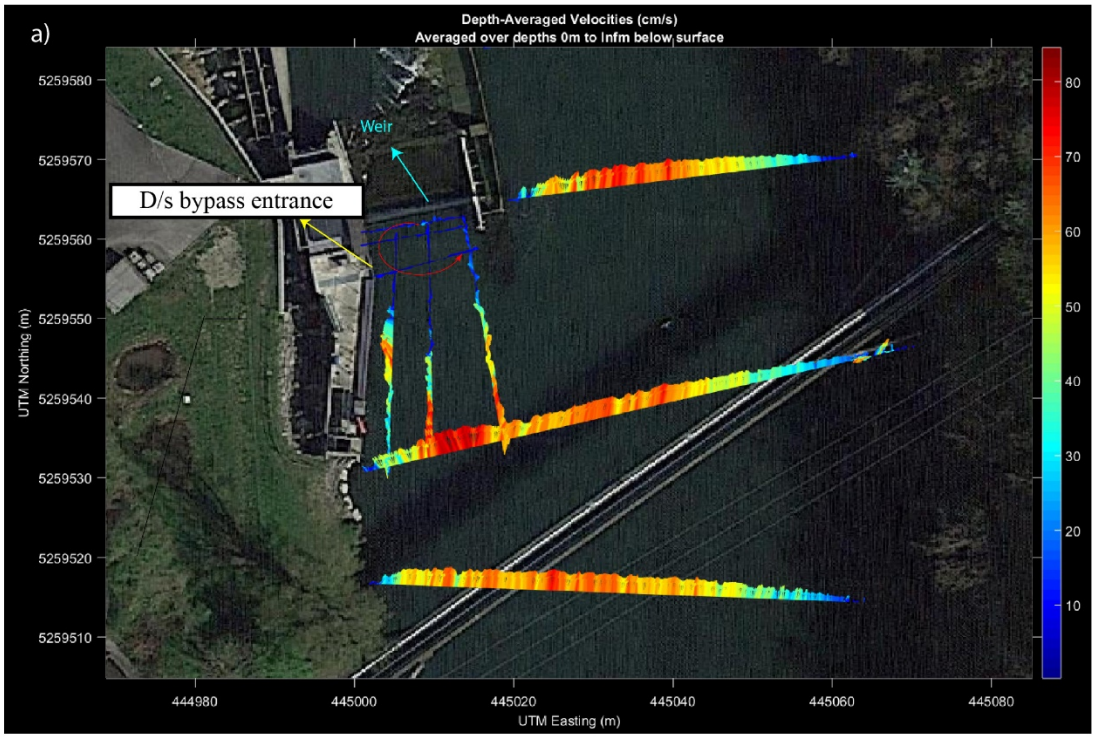

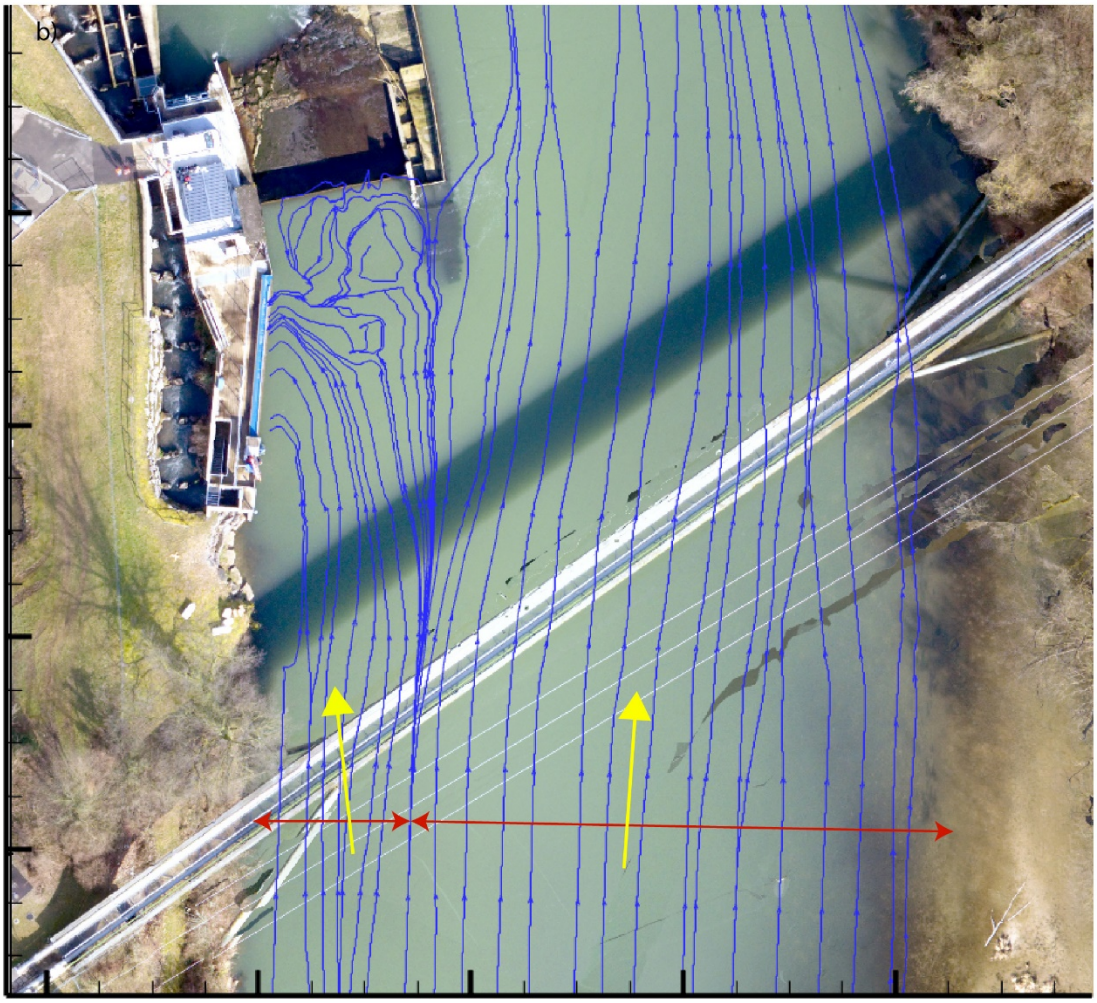

Figure 36: Depth-averaged velocity profiles (a) and streamlines (b) from ADCP measurements at HPP Schiffmühle in October 2018.

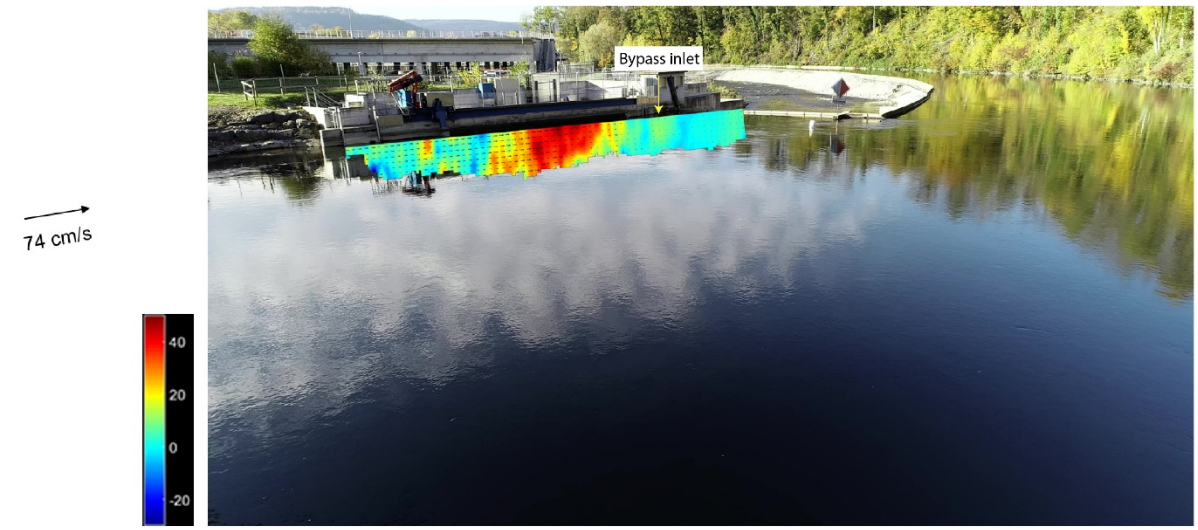

Figure 37: Velocity distribution along the HBR-BS in October 2018.

a)

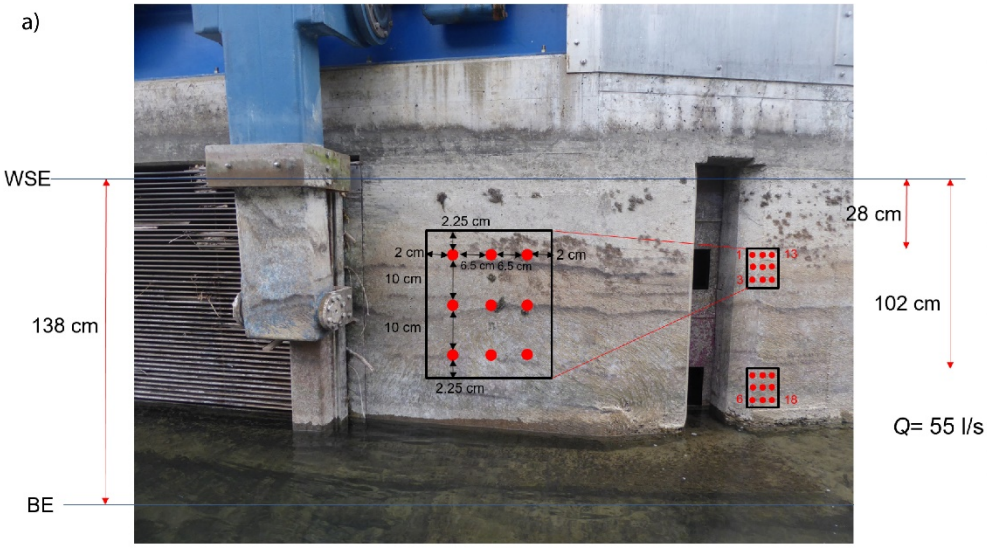

Point	Velocity (m/s)
1	0.66
2	0.72
3	0.70
4	0.66
5	0.73
6	0.64
7	0.65
8	0.66
9	0.75
10	0.75
11	0.72
12	0.66
13	0.65
14	0.63
15	0.52
16	0.48
17	0.63
18	0.70

b)

Figure 38: Velocity measurement points inside the bypass and velocity data (a) and average velocity in front of the bypass (b).

3.3.3.2 Hydraulics (AIV)

Figure 39 shows the resulting time-averaged surface velocity field. Note that according to Le Coz et al. (2010), depth-averaged velocities can be estimated by multiplying the surface velocity by factors of between 0.79 and 0.89, with a central value close to 0.85. Figure 40 presents the corresponding streamlines. It becomes obvious how the main flow is deflected to the outer bend of the headrace channel. The main flow must be accompanied by a strong streamwise-clockwise rotating secondary current that dives down a few meters before it reaches the right bank. There, a smaller streamwise-anticlockwise rotating secondary current is indicated by much slower flow velocities. The turbine approach flow upstream of the HBR-BS at the residual flow HPP has surface flow velocities of around 0.6–0.7 m/s, with the streamlines being deflected towards the turbine only a few meters upstream of the horizontal bar rack, which is in a good agreement with ADCP data (Figures 35a and 36b). The reach of the residual flow can be subdivided into two parts: (i) The area around the fish pass is affected by the turbine outlet of the residual flow power plant with surface velocities slightly above 1.0 m/s and (ii) the transverse ground sill downstream of the nature-like fish pass entrance that retains the water and slows down the surface velocity to 0.6–0.7 m/s. Downstream of the ground sill the flow is quite inhomogeneous and locally reaches surface velocities of up to 2.0 m/s in maximum.

Unfortunately, some areas show misleading flow velocities that obviously do not represent reliable flow physics. They are exemplarily highlighted in Figure 39. There are multiple reasons for this noise, such as a lack of seeding, white water, sun reflections, and higher riparian vegetation apparently moving with the moving camera position. Currently, VAW develops adequate techniques to avoid such noise directly during the video recording and to filter out falsified velocity vectors afterwards. As wrong velocity vectors in AIV are, in tendency, smaller than the real velocity, falsified time-averaged velocities are typical too low. Thus, local velocities have to be compared with neighboring velocities every time, and, in case of doubts, faster velocities are supposed to be closer to real–world situations.

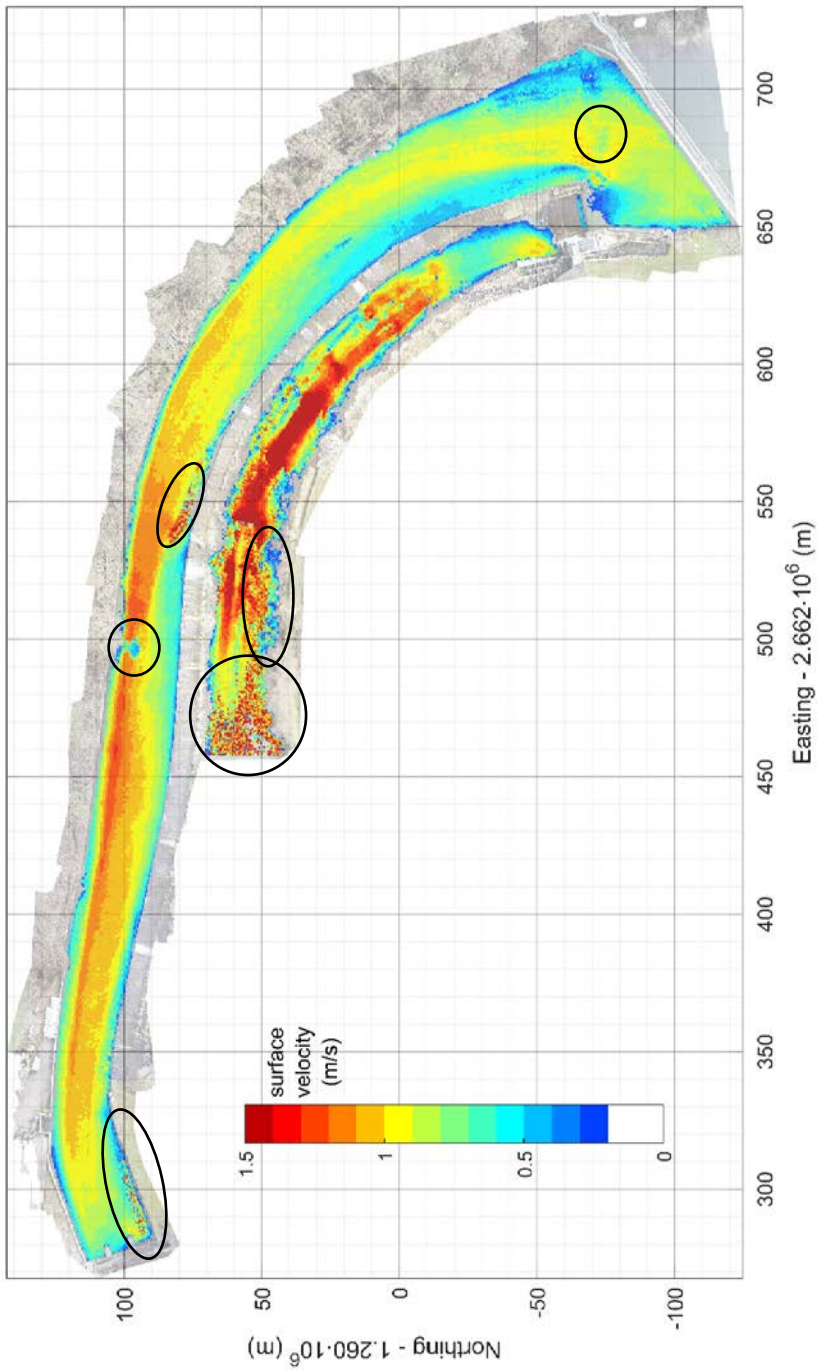

Figure 39: Geo-referenced surface velocity field measured using AIV on 2018/03/13 between 11:00-11:45 at a flow discharge of 71–72 m^3/s, with exemplary areas of misleading (noisy) velocity data highlighted by black ellipses

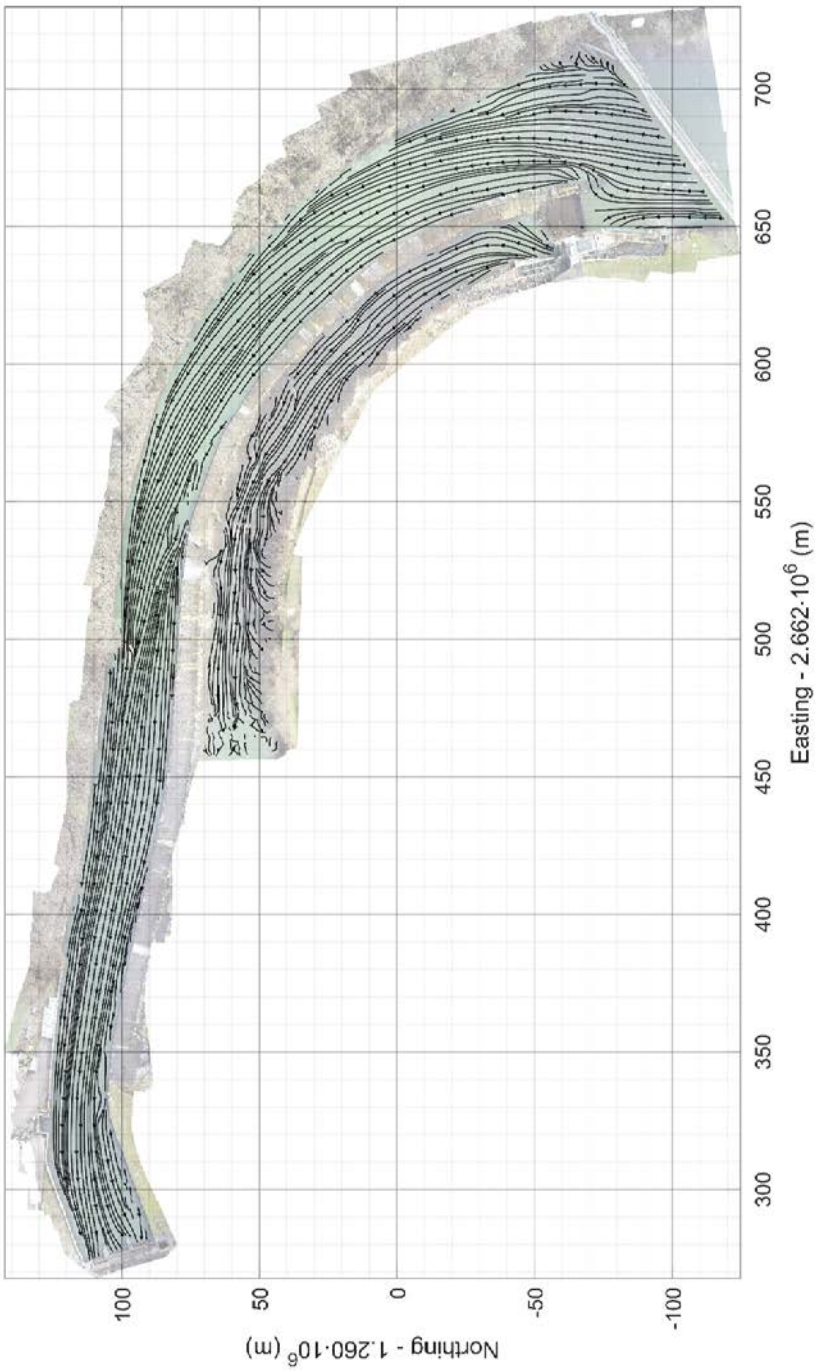

Figure 40: Geo-referenced surface velocity streamlines computed from AIV results

3.3.3.3 Fish monitoring

Figure 41 presents an overview of all tagged fishes. The range of the total length was from 82 to 900 mm (median 130 mm).

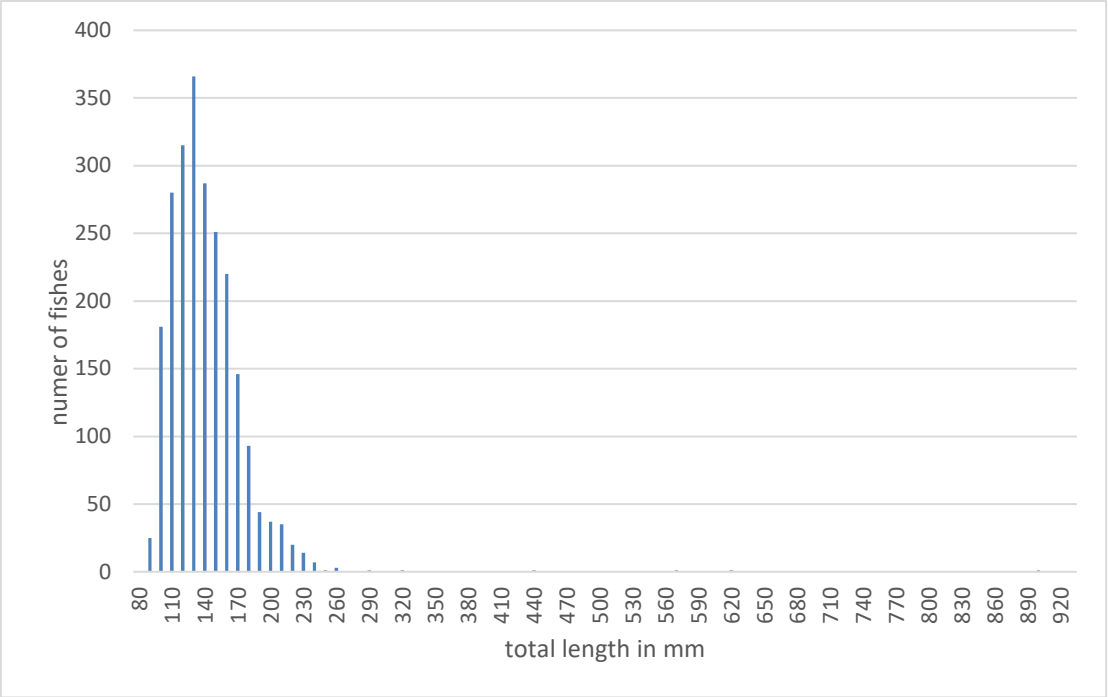

Figure 41: Total length of tagged fishes (N=2’331) belonging to 17 fish species. Only 5 individuals were larger than 300 mm.

Between 28 September 2017 and January 6 2019 251’570 detections were registered at the installed antennas. In Table 8 an overview of the detected fishes in the fish pass is presented. 1’601 of the tagged fishes (68.7 %) were detected. This can be considered as a very high rate. 1’280 tagged fish (54.9 %) successfully ascended the fish pass. Barbel prefer the entrance of the vertical-slot pass, while chub, roach and dace prefer to enter in the nature-like pass.

Additional analysis showed that for all fish species together the attraction efficiency (42.5 %) of the nature-like fishway was higher than in the vertical slot pass (31.6 %). However, the entrance efficiency in the vertical slot pass was with 98.8 % distinctly higher than in the nature-lake pass (86.5 %). On the other hand the passage efficiency for the vertical slot and the nature-like pass was very similar (≈ 80 %). Passage efficiency was calculated by dividing the number of fish that exited the fish pass by the number that was detected at the second antenna at the entrance.

Concerning the downstream migration, only one of the tagged fish was registered in the bypass. As shown in section 3.3.3.2, the re-circulation zone, low velocities between the weir and the bypass inlet compared to high flow velocity at the turbine intake as well as low velocities inside the bypass make it difficult for fish to find the bypass. This problem needs considerable attention. However, additional results from the year 2019 have to be included. In 2019 special downstream migration experiments will be carried out.

Table 8: Fish monitoring results

Species	N tagged	N detected	% detected	N ascended in vertical slot pass	N ascended in nature-like pass	Passage efficiency whole fish pass %
eel	1	1	100	1	0	100
chub	371	221	59.6	43	135	85.2
Brown trout	2	1	50	0	0	0
barbel	985	644	65.4	334	186	85.4
perch	131	86	65.6	16	40	69
gudgeon	5	1	20	0	0	0
bullhead	3	0	0	0	0	0
dace	81	73	90.1	6	46	85.9
carp	1	0	0	0	0	0
bleak	102	74	72.6	25	29	79.2
nase	5	3	60	0	2	100
roach	257	210	81.7	14	153	90.3
rudd	2	1	50	0	0	0
tench	2	0	0	0	0	0
spirlin	379	283	74.7	147	84	84.1
pumpkinseed	3	3	100	2	1	100
total	**2331**	**1601**	**68.7**	**588**	**676**	**84.6**

3.3.3.4 Hydraulics (Numerical modelling)

Results from 3D hydraulic modelling are foreseen in 2019 and will serve as important input to the habitat modelling.

3.3.4 Conclusions & Outlook

We documented the current situation and investigated the hydraulics, bathymetry and fish guidance efficiency of HBR-BS at HPP Schiffmühle by means of field monitoring and 3-D numerical modelling in the area near the powerhouse, and weir. The monitoring comprise:

- characterization of the flow field and river bathymetry using ADCP
- 3D numerical simulation
- survey of the fish movements using PIT-tagging technique

High resolution 3D velocity as well as bathymetry measurements were conducted using an Acoustic Doppler Current Profiler (ADCP) mounted on a high-speed remote control boat in March and October 2018. The ADCP data are used to construct the 3D numerical model of the HPP and calibrate and validate the model. Fish have been monitored at HBR-BS and both technical and nature-like fish passes using the PIT-tagging technique since 2017. The key results of these works include:

1) River bathymetries were mapped in March and October 2018 and used in 3D numerical model

2) Gravel replenishment from the headrace channel into the residual flow reach as sediment connectivity measure was done and its effects are quantified
3) Both ADCP and AIV velocity measurements indicate that most fish in the river are expected to follow the main stream towards the headrace channel while a small portion swims towards the HPP.
4) The attraction flow to the bypass for downstream migration seems inefficient and a re-circulation zone possibly affects fish searching the bypass entrance.
5) No fish was detected in the bypass confirming the poor velocity field around the bypass
6) Clogging of the bypass pipe is a problem affecting the bypass discharge and velocity
7) the downstream bypass system needs optimization
8) Both the technical and natural upstream fishways function efficiently

Based on the present results, we plan to conduct ADCP measurements in 2019 again. Moreover, fish monitoring will be continued in 2019. Numerical model results for various discharge scenarios will be available in 2019. Furthermore, optimization of bypass geometry and hydraulics, and options of possible new bypass locations such as at the left side of the weir will be numerically studied to improve the bypass attraction flow and hence fish guidance efficiency of HBR-BS.

3.4 Habitat modelling (SJE, TUT)

The attraction flow from the fish pass outlets will be investigated with the habitat simulation system CASiMiR. A Lateral Line Probe (LLP) will be used to study fish habitats and potential migration pathways using machine learning algorithms which are based on a spectral analysis of the recorded narrowband pressure fields. The results from LLP and CASiMiR will be compared.

To characterize the relationship between the local hydrodynamic conditions in the fishway outlet flow ("attraction flow") and the spatial distribution of local flow variables, an artificial lateral line probe (LLP) as well as an acoustic Doppler velocimeter (ADV) are used and are shown in Figure 42. The use of the ADV provides velocity data comparable to available studies on attraction flows, and the use of a LLP provides body-oriented differential pressure fluctuations in order to explore the additional data gained using the lateral line probe (higher sampling rate and distributed sensing). Compared to point velocity measurements delivered by ADV, LLP captures the physical metrics (body-oriented pressure gradients) which may be closer to the "fish's perspective".

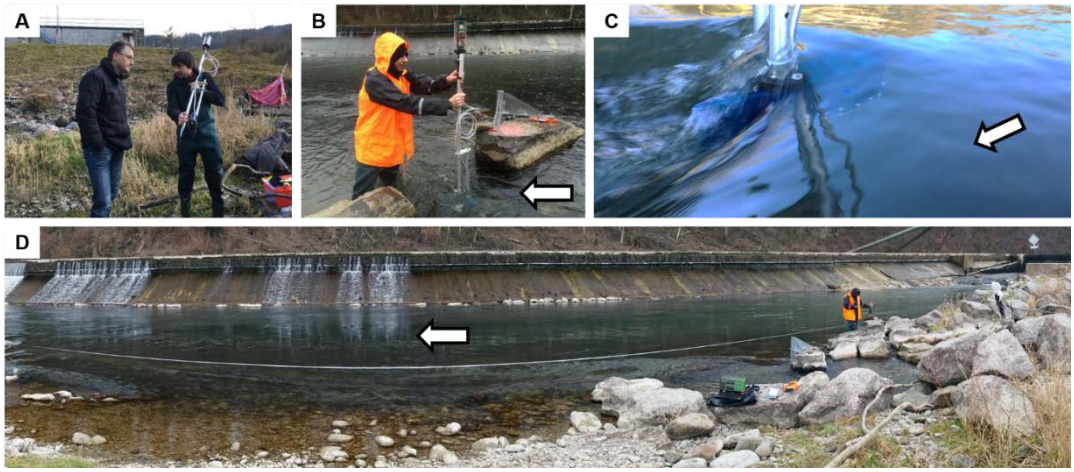

Figure 42: A) Lateral line probe can be used easily, and requires a short field training. B) The LLP measurements can be made directly in the attraction flow jet. C) Close-up view of the LLP near the top of the water column, illustrating the water flow around the probe body. D) A measuring tape extended in the field along the jet core facilitates reproducible measurement locations for future studies using ADV or LLP.

3.3.1 Data

Data are collected as pressure time series from the ADV (velocity U,V,W) and LLP (differential pressure sensor readings, water temperature, water depth). All data files are stored on a secured server and shared with FITHydro project partners as required in the consortium agreement.

3.3.2 Methodology

CASiMiR and LLP

The results of the bathymetric and hydrodynamic model are the basis for the analysis of fish migration; yet they are currently not available (as of January 2019). The telemetric investigations in the test case Schiffmühle do not deliver tracks of fish approaching the fish pass, but the fish entering and leaving the fish pass are counted. Thus, it is not possible to use the telemetric data for the development of CASiMiR migration which aims on the assessment of attraction flow. The test case Schiffmühle will instead be used for testing the migration model, which is developed based on data from the test case Altusried, Iller, where fish tracks are available. The intention is to find relations between the flow rates that provide good conditions in terms of attraction flow and the number of fish entering the fish ladder from downstream.

The lateral line probe measurements were performed by TUT and SJE on March 13 and 14, 2018 along the center of the jet core at the bottom, mid-depth and top of the water column (Figure 43). This was done for two reasons: 1) Some fish species are known to be bottom-oriented, but there is no available information on the hydraulic conditions in-situ near the bottom for attraction flow studies. 2) 2D models cannot capture the vertical distribution of the velocity and it is therefore important to determine the physical differences between the bottom, mid (velocity in 2D models is depth-averaged and corresponds roughly to this region), and top of the water column.

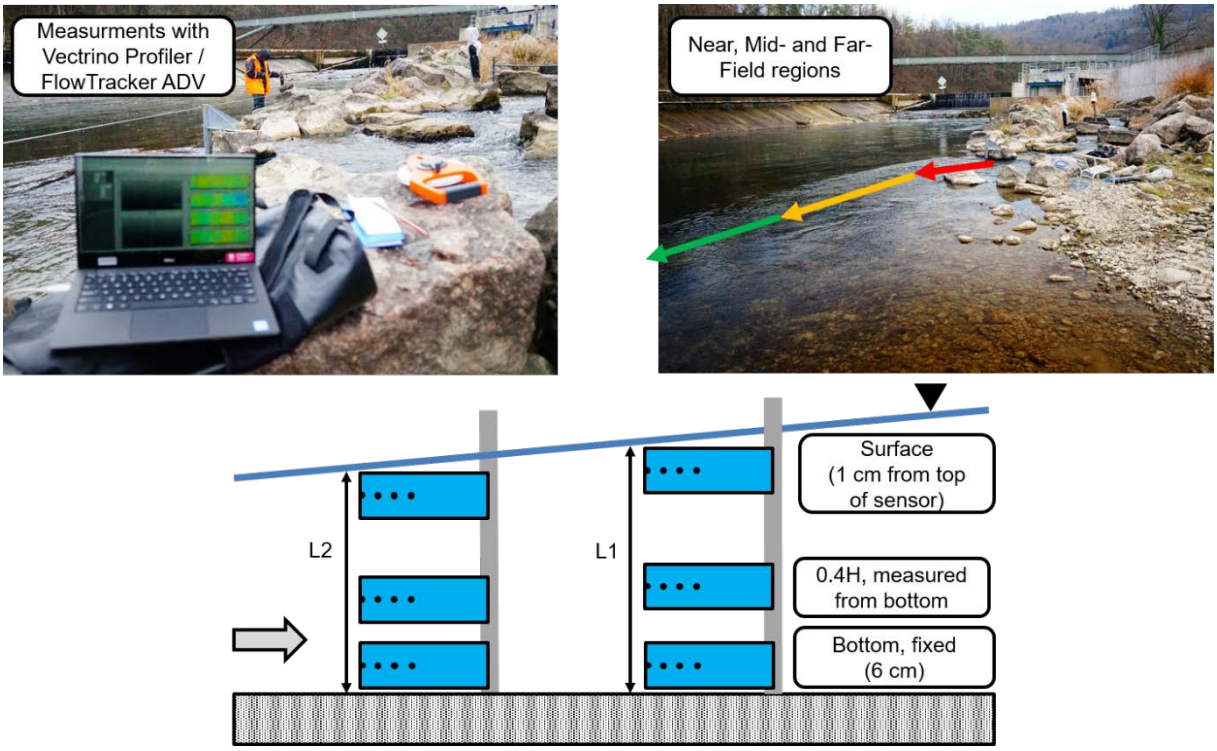

Figure 43: Top images show LLP and ADV measurement locations at the Schiffmühle case study site which correspond to the near, mid- and far-field regions of the jet core. Lower image depicts the vertical measurement locations for the LLP and ADV in order to capture the hydrodynamic conditions of the jet core at the bottom, middle and top of the water column.

3.3.3 Results

Data processing from the LLP is currently ongoing. Based on our work using the LLP as part of the live fish behaviour studies in Portugal, as series of best-performing LLP pressure metrics has been compiled and will be compared to the ADV data and are listed in Table 9.

Table 9 : Pressure-based variables from LLP measurements.

Variables	Equation
Mean pressure[1]	$\overline{p}_i = \frac{\sum_{j=1}^{n} p_{i,j}}{N}$
Mean fluctuations[1]	$\overline{p}'_i = \frac{\sum_{j=1}^{n} \left\lvert p_{i,j} - \overline{p}_i \right\rvert}{N}$
Mean front pressure ($\overline{p}_{12}$)	$\overline{p}_{12} = \frac{\sum_{j=1}^{n} p_{1,j} + p_{2,j}}{N}$
Mean pressure ($\overline{p}_{1-6}$)	$\overline{p}_{1-6} = \frac{\sum_{j=1}^{n} \frac{\sum_{k=1}^{6} p_{k,j}}{6}}{N}$
Mean front fluctuations ($\overline{p}'_{12}$)	$\overline{p}'_{12} = \frac{\overline{p}'_1 + \overline{p}'_2}{2}$
Mean fluctuations ($\overline{p}'_{1-6}$)	$\overline{p}'_{1-6} = \frac{\sum_{i=1}^{n} \overline{p}'_i}{N}$
Mean front pressure asymmetry ($\Delta\overline{p}_{12}$)	$\Delta\overline{p}_{12} = \frac{\sum_{j=1}^{n} \left(p_{1,j} - p_{2,j} \right)^2}{N}$
Mean pressure asymmetry ($\Delta\overline{p}_{1-6}$)	$\Delta\overline{p}_{1-6} = \frac{\sum_{k}^{m} \frac{\sum_{j=1}^{n} \left(p_{2k-1,j} - p_{2k,j} \right)^2}{N}}{M}$
Mean front fluctuations asymmetry ($\Delta\overline{p}'_{12}$)	$\Delta\overline{p}'_{12} = \frac{\sum_{j=1}^{n} \left(p'_{1,j} - p'_{2,j} \right)^2}{N}$
Mean fluctuations asymmetry ($\Delta\overline{p}'_{1-6}$)	$\Delta\overline{p}_{1-6} = \frac{\sum_{k}^{m} \frac{\sum_{j=1}^{n} \left(p'_{2k-1,j} - p'_{2k,j} \right)^2}{N}}{M}$

[1]Only for the variable definition above. Sensors are not considered individually.

3.3.4 Conclusion

Results for the forthcoming LLP evaluation will be published in the form of a peer-reviewed paper in 2019.

Results of the attraction flow assessment can only be delivered after the hydrodynamic model is available and after the migration model based on the correlation between fish tracks and hydrodynamic measurements and modelling from the test case Altusried will be available.

4 Reference

Atkinson, E. (1994a). Vortex-tube Sediment Extractors. I: Trapping Efficiency. *Journal of Hydraulic Engineering*, 120(10), 1110-1125.

Atkinson, E. (1994b). Vortex-tube Sediment Extractors. II: Design. *Journal of Hydraulic Engineering*, 120(10), 1126-1138.

Awasthi, A.K. (2001). Desanding for Small Hydro - An Innovative Approach. *Proceedings of the 2nd International Conference 'Silting Problems in Hydropower Plants'*, Bangkok, Thailand.

Bunte, K., Abt, S.R. (2001). Sampling surface and subsurface particle-size distributions in wadable gravel- and cobble-bed streams for analyses in sediment transport, hydraulics, and streambed monitoring. *Gen. Tech. Rep. RMRS-GTR-74*. Fort Collins, CO: US Department of Agriculture, Forest Service, Rocky Mountain Research Station. 428 p.

Deliverable 2.2. of FIThydro (2019). Working basis of solutions, models, tools and devices and identification of their application range on a regional and overall level to attain self-sustained fish populations. https://www.fithydro.eu/deliverables-tech/

Detert, M., and Weitbrecht, V. (2013). User guide to gravelometric image analysis by BASEGRAIN. *Advances in science and research* (S. Fukuoka, H. Nakagawa, T. Sumi, and H. Zhang eds.), Taylor & Francis, London, 1789-1795.

Detert, M., Johnson, E.D., Weitbrecht, V. 2017. Proof-of-concept for low-cost and non-contact synoptic airborne river flow measurements. *International Journal of Remote Sensing* 38(8–10), 2780–2807. doi:10.1080/01431161.2017.1294782

Finstad, A.G., Einum, S., Forseth, T., Ugedal, O., 2007. Shelter availability affects behaviour, size-dependent and mean growth of juvenile Atlantic salmon. *Freshwater Biology* 52, 1710–1718. https://doi.org/10.1111/j.1365-2427.2007.01799.x

Flow Science, Inc (2014): FLOW-3D Version 11.0.3 – User manual

Flussbau AG (2017). Geschiebehaushalt Limmat, Geschiebedurchgängigkeit Streichwehre (Bedload balance Limmat, bedload conveyance of side weirs). *Technical Report* [unpublished, in German].

Forseth, T., Harby, A., Ugedal, O., Pulg, U., Fjeldstad, H.-P., Robertsen, G., Barlaup, B.T., Alfredsen, K., Sundt, H., Salveit, S.J., Skoglund, H., Kvingedal, E., Sundt-Hansen, L.E.B., Finstad, A., Einum, S., Arnekleiv, J.V., 2014. *Handbook for environmental design in regulated salmon rivers* (NINA temahefte No. 53). Norsk institutt for naturforskning.

Graham, D.J., Rollet, A.-J., Piégay, H., and Rice, S.P. (2010). Maximizing the accuracy of image-based surface sediment sampling techniques. *Water Resources Research*, 41(7), 1-12.

Gray, J.R., Laronne, J.B., Marr, J.D.G. (2010). Bedload-surrogate Monitoring Technologies, *US Geological Survey Scientific Investigations Report 2010-5091*. US Geological Survey: Reston VA.

Kzyzagorski, S., Gabl, R., Seibl, J. et al. (2016) Implementierung eines schräg angeströmten Rechens in die 3D-numerische Berechnung mit FLOW-3D. *Österr. Wasser- und Abfallw.* 68: 146. doi:10.1007/s00506-016-0299-2

Le Coz, J., Hauet, A., Pierrefeu, G., Dramais, G., Camenen, B. 2010. Performance of Image-Based Velocimetry (LSPIV) Applied to Flash-Flood Discharge Measurements in Mediterranean Rivers. *Journal of Hydrology* 349(1–2), 42–52. doi:10.1016/j.jhydrol.2010.05.049.

Meusburger, H. (2002): Energieverluste an Einlaufrechen von Flusskraftwerken. *VAW Mitteilungen* Nr. 179 (H.-E. Minor, ed.), ETH Zürich. http://people.ee.ethz.ch/~vawweb/vaw_mitteilungen/179/179_g.pdf

Mtalo, F. (1988). Geschiebeabzug aus Kanälen mit Hilfe von Wirbelröhren (Bedload diversion from channels with vortex tubes). *Report No. 58*, Hydraulic Research Institute Obernach, Technical University of Munich, Germany [in German].

Rickenmann, D., Turowski, J.M., Fritschi, B., Klaiber, A., Ludwig, A. (2012). Bedload transport measurements at the Erlenbach stream with geophones and automated basket samplers. *Earth Surface Processes and Landforms*, 37, 1000-1011.

Rickenmann, D., Turowski, J.M., Fritschi, B., Wyss, C., Laronne, J., Barzilai, R., Reid, I., Kreisler, A., Aigner, J., Seitz, H., Habersack, H. (2014). Bedload transport measurements with impact plate geophones: comparison of sensor calibration in different gravel-bed streams. *Earth Surface Processes and Landforms*, 39, 928-942.

Stähly, S., Friedrich, H., Detert, M. (2017). Size Ratio of Fluvial Grains' Intermediate Axes Assessed by Image Processing and Square-Hole Sieving. *Journal of Hydraulic Engineering*, 143(6): pages??.

Thielicke, W., Stamhuis, E. J. 2014. PIVlab – Towards User-Friendly, Affordable and Accurate Digital Particle Image Velocimetry in MATLAB. *Journal of Open Research Software* 2:e30. doi:10.5334/jors.bl

VAW (2001). Kraftwerk Schiffmühle (Hydropower plant Schiffmühle). *VAW-Report 4158*, ETH Zurich, Laboratory of Hydraulics, Hydrology and Glaciology (VAW), Switzerland [unpublished, in German].

VAW (2017). Wirbelröhre Kraftwerk Turgi (Vortex tube hydropower plant Turgi). *VAW-Report 4343*, Laboratory of Hydraulics, Hydrology and Glaciology (VAW), ETH Zurich, Switzerland [unpublished, in German].

Westerweel, J., Scarano, F. 2005. Universal outlier detection for PIV data. Experiments in Fluids 39(6), 1096–1100. doi:10.1007/s00348-005-0016-6

Wyss, C.R., Rickenmann, D., Fritschi, B., Turowski, J.M., Weitbrecht, V., Boes, R.M. (2016a). Measuring Bed Load Transport Rates by Grain-Size Fraction Using the Swiss Plate Geophone Signal at the Erlenbach. *Journal of Hydraulic Engineering*, 142(5): 04016003.

Wyss, C.R., Rickenmann, D., Fritschi, B., Turowski, J.M, Weitbrecht, V., Boes, R.M. (2016b). Laboratory flume experiments with the Swiss plate geophone bed load monitoring system: 1. Impulse counts and particle size identification. *Water Resources Research*, 52, 7744-7759.

Wyss, C.R., Rickenmann, D., Fritschi, B., Turowski, J.M, Weitbrecht, V., Boes, R.M. (2016c). Laboratory flume experiments with the Swiss plate geophone bed load monitoring system: 2. Application to field sites with direct bed load samples. *Water Resources Research*, 52, 7760-7778.

Zabah E. 2018. *KWS_26-03-2018.zip, KWS_26-03-2018ply.zip*. Regionalwerke Baden AG (pers. communication)